GL-TR-89-0330

COPY

(4)

AD-A220 771

The Phase-Screen Method for Elastic
Wave and Seismic Discrimination

Mark D. Fisk
Gary D. McCartor

Mission Research Corporation
735 State Street
P.O. Drawer 719
Santa Barbara, CA 93102-0719

15 December 1989

Scientific Report No. 1

APPROVED FOR PUBLIC RELEASE; DISTRIBUTION UNLIMITED

GEOPHYSICS LABORATORY
AIR FORCE SYSTEMS COMMAND
UNITED STATES AIR FORCE
HANSCOM AIR FORCE BASE, MASSACHUSETTS 01731-5300

DTIC
ELECTE
APR24 1990
S B D

90 04 23 040

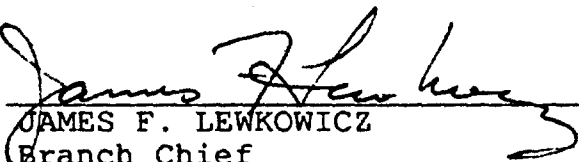This technical report has been reviewed and is approved for publication.

JAMES F. LEWKOWICZ
Contract Manager
Solid Earth Geophysics Branch
Earth Sciences Division

JAMES F. LEWKOWICZ
Branch Chief
Solid Earth Geophysics Branch
Earth Sciences Division

FOR THE COMMANDER

DONALD H. ECKHARDT, Director
Earth Sciences Division

Best Available Copy

REPORT DOCUMENTATION PAGE

1. AGENCY USE ONLY (Leave blank)	2. REPORT DATE	3. REPORT TYPE AND DATES COVERED
	15 December 1989	Scientific Report No. 1 2/89 - 2/90

4. TITLE AND SUBTITLE	5. FUNDING NUMBERS
The Phase-Screen Method for Elastic Wave and Seismic Discrimination	PE 62714E PR 7A10 TA DA WU BE
6. AUTHOR(S) Mark D. Fisk Gary D. McCartor	Contract F19628-89-C-0040

7. PERFORMING ORGANIZATION NAME(S) AND ADDRESS(ES)	8. PERFORMING ORGANIZATION REPORT NUMBER
Mission Research Corporation 735 State Street P.O. Drawer 719 Santa Barbara, CA 93102-0719	

9. SPONSORING/MONITORING AGENCY NAME(S) AND ADDRESS(ES)	10. SPONSORING/MONITORING AGENCY REPORT NUMBER
Geophysics Laboratory Hanscom AFB, MA 01731-5000 Program Manager: James Lewkowicz/LWH	GL-TR-89-0330

11. SUPPLEMENTARY NOTES

12a. DISTRIBUTION/AVAILABILITY STATEMENT	12b. DISTRIBUTION CODE
Approved for public release, distribution unlimited	

13. ABSTRACT (Maximum 200 words) The phase-screen method to compute elastic vector wave propagation in three-dimensional heterogeneous media is developed, accounting for the difference in phase velocities of the transverse and lognitudinal polarizations. The method replaces the heterogeneous medium with a homogeneous one and a set of phase screens. Between the screens the displacement is propagated by the uniform elastodynamic wave equation. The phase of each polarization of the wave, accumulated from propagating in the z-direction, is corrected at the screens to account for inhomogeneities. Only forward propagation is included in the analysis. A criterion is derived to determine the number of phase screens to be used. The energy fluxes of the S and P waves are also computed. We find that energy conservation requires special consideration for application of the method to vector waves. The method is tested on a two-dimensional problem whose exact solution is also computed. The primary application of the method is to compute vector wave propagation in random media for the purpose of treaty monitoring. In particular, we demonstrate how P-S conversion and S_H - S_V ratios may be efficiently computed for realistic media by employing the phase-screen method based on statistical modeling.

14. SUBJECT TERMS			15. NUMBER OF PAGES
Phase Screen	Energy Flux	S-wave	82
Random Media	P-wave	Regional Phases	**16. PRICE CODE**

17. SECURITY CLASSIFICATION OF REPORT	18. SECURITY CLASSIFICATION OF THIS PAGE	19. SECURITY CLASSIFICATION OF ABSTRACT	20. LIMITATION OF ABSTRACT
Unclassified	Unclassified	Unclassified	SAR

TABLE OF CONTENTS

iii

LIST OF ILLUSTRATIONS

LIST OF ILLUSTRATIONS (CONCLUDED)

THIS PAGE IS INTENTIONALLY LEFT BLANK

SECTION 1

INTRODUCTION

In this report we shall describe a method for calculating the propagation of elastic waves. The method, the phase-screen method, has some relation to WKBJ and other high frequency methods; the details are quite different. The wave equations of elastodynamics are solved exactly, the approximation being made on the medium through which the waves propagate rather than on the solutions to the dynamical equations themselves. While the method can be used to calculate the propagation through a complex medium with a known spatial distribution of elastic parameters (an example is given below), probably the most common use of the method in previous work has been to study the propagation of waves in stochastic media where only statistical properties of the media are known; it is this last application we have in mind here.

The method is not new. It has been used for many years by astronomers to estimate the effects of the atmosphere on the propagation of starlight, Ratcliffe [1956], by engineers to study the effects of structure on the propagation of signals from communication satellites, Knepp [1983], by acoustical engineers to study the propagation of sound in the ocean, Flatté [1983] and Martin and Flatté [1988], and for other purposes. All of the past studies of which we are aware have considered only the case of scalar waves. Here we shall formulate the problem for the case of vector elastic waves; indeed it is the interconversion of transverse and longitudinal components that provides a major focus of the study.

Consider a simple plane wave ($k = w/c$), where a harmonic time dependence of frequency w is assumed propagating in a medium with sound speed c.

$$\phi = e^{i\frac{w}{c}z} .$$

(1)

If we use that solution as an approximation in a medium with sound speed c', we find that at any fixed z the relation between the approximate solution, ϕ, and the exact solution, ψ, is just a phase

$$\psi = e^{iw\frac{c-c'}{cc'}z}\phi.$$

(2)

1

In this simplest example the effect of a velocity anomaly is just to advance or retard the phase of the wave; that is the central approximation in the phase-screen method: we assume that the effect of velocity anomalies is to retard or advance the phase of the wave.

Now consider the situation depicted in figure 1. A wave is propagating from $z = 0$ to $z = \Delta z$ through a medium whose mean sound speed is $\bar{c}$ with velocity anomalies $\delta c(x, y, z)$ present. Our first approximation is that the effect of the anomalies is to multiply the solution at Δz by an x-y-dependent phase factor given by

$$\exp\left(i\Delta(x,y)\right) = \exp\left[-i\frac{w}{\bar{c}}\Delta z + iw \int_0^{\Delta s} \frac{dz'}{\bar{c} + \delta c(x, y, z')}\right]. \tag{3}$$

Thus the problem shown in figure 1 has been replaced by that shown in figure 2 where the propagation from 0 to $z = \Delta z_-$ is through a medium with a constant sound speed $\bar{c}$. The result is then multiplied by a phase factor given by (3) to obtain the wave at $z = \Delta z_+$.

To this point we have considered the case where at $z = 0$ we had a simple plane wave but for more complex cases where the solution at $z = 0$ is a function of x and y we will use the same procedure of figure 2: propagate through a uniform medium to $z = \Delta z_-$ then correct the phase at $z = \Delta z_+$. With that generalization we have the possibility of repeating the procedure, inserting phase screens at other larger values of z. That possibility brings up the other approximation we must make: we must make the problem parabolic; that is to say, we wish to have a formulation such that the value of the wave function at some fixed z determines the value at larger z's. Since the wave equation is second order in each spatial variable that is not the usual case; usually an initial value problem would require specification of two functions (e.g. ϕ and $\partial_z \phi$) at a fixed z in order to determine the solution. As an alternative we can specify the value of the function on two planes corresponding to different values of z. What we shall do is a variant of this last possibility: we shall use the value of the function at $z = 0$ and impose outgoing boundary conditions at $z \to \infty$. That formulates a well-posed boundary value problem and allows us to solve for the function at Δz_+. A standard way to solve such a problem is to decompose the value of the function at $z = 0$ into a set of plane waves whose propagation vector points into the right-hand cone. Thus we make the problem parabolic by a procedure which can be stated one of two equivalent ways: we use the value of the function at $z = 0$ plus a boundary condition at $z \to \infty$; or, we use the value of the function at $z = 0$ plus the assumption of forward propagating waves.
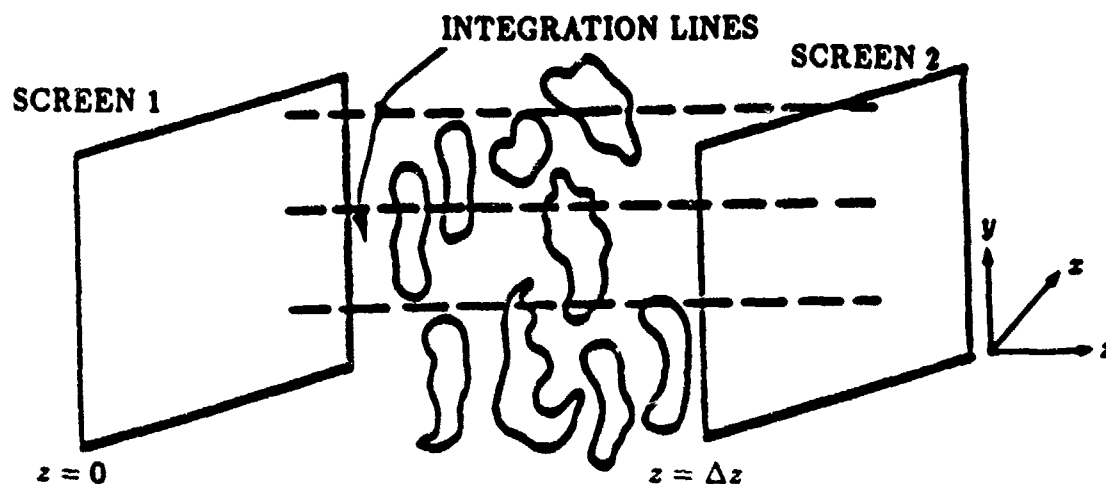
Figure 1.   Propagation of the wave through a segment of inhomogeneous medium alters the phase of the wave as a function of position due to the velocity anomalies in the medium.
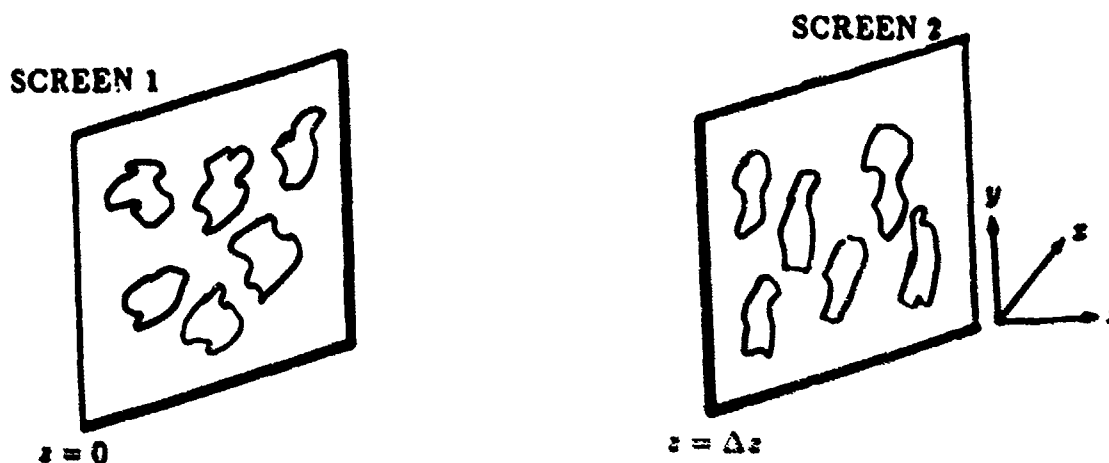
Figure 2.   The phase-screen method replaces the inhomogeneous segment with a uniform segment and a pair of phase screens. The integrated phase defect of the segment is projected onto the second screen.

3

The approximations just described allow us to take an initial value for the wave function and propagate the wave through an arbitrary number of phase-screens to find its value at any z. Furthermore the extension to vector elastic waves is obvious: given the displacements at $z = 0$ we can uniquely decompose them onto the set of S and P waves which have propagation vectors pointing into the right-hand cone. We can thus evaluate the displacements at $z = \Delta z_-$, modify them at $z = \Delta z_+$ with separate phase factors using the appropriate phase velocity for each, and then propagate the wave, according to the uniform vector wave equation, to the next phase screen where the process is repeated. Detailed formulas are given in the next section.

We should remark here about the relation between the explanation of the phase-screen method we have just presented and another, slightly different discussion the reader may have seen elsewhere. Sometimes the starting point for explanation of the phase-screen method is to write the field as

$$\phi(x,y,z) = \psi(x,y,z)e^{ik_s z}, \tag{4}$$

where

$$k_s = \frac{\omega}{\bar{c}}, \tag{5}$$

and ψ is a slowly varying function of z. This leads to the replacement of the wave equation

$$\nabla^2 \phi + \frac{\omega^2}{c^2}\phi = 0 \tag{6}$$

with the "parabolic wave equation"

$$\left[\nabla_\perp^2 + 2ik_s\frac{\partial}{\partial z} + \left(\frac{\omega^2}{c^2} - \frac{\omega^2}{\bar{c}^2}\right)\right]\psi(x,y,z) = 0, \tag{7}$$

where

$$\nabla_\perp^2 = \partial_x^2 + \partial_y^2. \tag{8}$$

4

The problem is thus made parabolic by modifying the dynamical equation to be first order in z so specifying ϕ at one value of z determines the solution.

In addition to this modification of the wave equation, the phase factors that correct for the velocity anomalies of the medium are generally taken to be independent of k_x and k_y. These approximations are justified for either scalar or vector waves provided k_x and k_y are in fact small compared to $w/\bar{c}$, where $\bar{c}$ generically represents either of the two average phase velocities for the vector wave case. By dimensional analysis, k_x and k_y are inversely proportional to the length scales in the plane normal to the z-axis. Thus if these lengths are large enough, the approximation is valid. We have found, based on the comparison of the phase-screen method with an exact solution, which we describe below, that using the full uniform wave equation, and phase factors that depend on k_x and k_y, allows us to accurately calculate propagation for slightly smaller structures. Certainly larger structures will lead to better results since waves propagating at large oblique angles are apt to induce backscattering, which is not accounted for in the formalism. For large enough structures, the parabolic approximation is recovered by expanding our results for small k_x, k_y.

A slight variant of the method has been used before in seismology. Haddon and Huseby [1978] used what amounts to a phase-screen calculation combined with a stationary phase (ray) approximation, Mercier [1961], to calculate propagation into the NORSAR array. The combination of phase-screen and stationary phase approximation produces the thin lense approximation of geometrical optics. They considered only P waves. The method described here could be used for the same situations including both S and P waves.

Until now we have simply generalized the phase-screen approximation for scalar waves in an obvious way to account for the two phase velocities, and avoided making the parabolic approximation to the wave equation. Regardless of whether we employ the parabolic approximation or not, this leads to significant consequences regarding the conservation of energy. Certainly if a wave is multiplied by an overall phase, energy will be conserved. However, if individual contributions to the total wave are multiplied by different phases, the energy of the subsequent wave will not be equal to the energy of the original wave; interference terms will result. Indeed this is the case if we naively multiply the S and P waves by different phase factors. Although the violation of energy conservation is quite small at each phase screen using parameters for which we expect the method to be valid, the cumulative result of propagating the wave over distances of say 1000 km is significant. It is also particularly disconcerting that energy may be gained as well as lost.

5

To remedy this problem while maintaining the spirit of the method, we modify the method described thus far in the following way. First, we find the recursion relations that express the Fourier coefficients of the wave after it has passed through the screen in terms of the Fourier coefficients of the wave before the screen and the phase factors which modify the wave at the screen. The recursion relations are conveniently expressed in terms of a matrix multiplying the column vector of old coefficients to produce the column vector of new coefficients. These are vectors and matrices in the space of Fourier modes, not spacetime. Thus if V, V', and U are the old vector, the new vector, and the recursion matrix respectively, then

$$V'_m = U_{mn}V_n, \tag{9}$$

where we are employing the convention that repeated indices are summed over.

In principle the vector space we are dealing with is infinite dimensional, however, for practical computational purposes it must be truncated. The second step of the algorithm is to neglect the evanescent modes, keeping only the finite number of modes with harmonic z-dependence. This is reasonable for two reasons. First, we are interested in propagation distances for which the evanescent modes have been exponentially damped. And second, as we will show later, the evanescent modes do not contribute to the energy. In fact, the energy flux in the z-direction averaged over time and the coordinates perpindicular to the z-axis is simply the norm squared of the vector of Fourier coefficients corresponding to the modes that propagate.

The condition that energy is conserved across the phase screen is that U be a unitary matrix, *i. e.* it must preserve the length of the vector. This, however, is not the case when we naively multiply the S and P waves by individual phases, although for cases of interest it is almost unitary in the sense that its eigenvalues are almost of unit modulus, and the commutator of U with its adjoint has small entries. [1] Thus the third step of the algorithm is to make U unitary. The procedure used to modify the matrix will be described later in full detail.

We are now ready to move on to the details of the method, which will be organized as follows. In chapter 2, we present the general theoretical details of the 3D method. In particular, the general recursion relations that determine the Fourier coefficients of the succeeding wave in terms of the Fourier coefficients of the previous wave and the Δ-phases, *i. e.* the phases that modify the wave at the phase screen, are

---

[1]The necessary and sufficient conditions for a matrix to be unitary is that it commute with its adjoint and have unit modulus eigenvalues.

derived. With these recursion relations, an incoming source wave may be iteratively propagated through an arbitrary number of phase screens.

Also in chapter 2, we derive a general criterion to specify the number and spacing of phase screens to be used. The basic idea behind the criterion is that for fixed observation distance the phase-screen solution should converge to a fixed answer as the number of phase screens are increased. This is analogous to the calculus of integrals where as the interval is broken up into smaller and smaller regions the convergent limit is obtained. [2] To optimize computer time, we are interested in finding the marginal number of phase screens needed such that the answer converges to its asymptotic limit to within a fixed tolerance. The criterion is cast in the form of a Cauchy condition for sequences; two successive terms in the sequence are compared to determine how well the sequence is converging.

Finally in chapter 2, the time-averaged energy flux is computed in terms of the Fourier coefficients of the phase-screen solution. As mentioned previously the displacement decomposes naturally in terms of S and P waves; each mode is represented by a Fourier coefficient. This allows the energy contribution from each mode to be calculated. These quantities will be useful to determine the magnitude of P to S conversion, and vice versa, and which features of the medium dictate the magnitude of the conversion. Included in this discussion is the matrix formulation of the method, and a detailed description of the numerical procedure for making the recursion matrix unitary.

In chapter 3, we test the applicability of the method for a 2D sample problem whose exact solution is also calculated. This provides a check on the method and some guidelines to follow concerning the range of parameters for which the approximation is valid. This will help in the extrapolation of the phase-screen method to problems whose exact solutions cannot be obtained. The actual comparison is made in two ways. First, by plotting the cartesian components of both solutions for various parameters of the problem, and second, by computing the average of the norm of the difference of the two wave vectors. To perform these comparisons more efficiently, we first determine the marginal number of phase screens needed such that adding additional phase screens for fixed observation distance does not significantly improve the answer.

Chapter 3 is concluded with an examination of energy flux conversion for the test problem. Using a single phase screen, we extremize the S to P and P to S conversion as a function of the ratio of the width of the regions to the free space

---

[2]Indeed the limit as the distance between phase screens approaches zero has some resemblence to the path integral approach to wave propagation, neglecting backscattering, Dashen [1979] and Flatté [1983].

wavelength for various ratios of the two sound speeds. This will indicate which wavelengths, or equivalently what structure sizes, induce the most conversion, and how it depends on the velocities.

In chapter 4, the phase-screen method for random media is discussed, and the details of some specific examples are given. We are primarily interested in the rate of conversion when the medium is characterized by random velocity fluctuations, and how it depends on the frequency, the correlation length, the velocity fluctuations, the distance of propagation, and the type of initial disturbance. In particular, we model a two dimensional random medium with only one length scale by randomly aligning the phase screens and ensemble averaging over realizations. Each realization is specified by a set of computer generated psuedo-random numbers that determine by how much each phase screen gets shifted. We find that the rate of energy conversion has a robust dependence on the magnitude of the velocity fluctuations and the structure size, and to a lesser extent on the frequency and whether the initial disturbance is a P wave or an S wave. We also find that the energies tend to constant equilibrium values after propagating a distance far enough, depending on the parameters which determine the rate of conversion, and that the equilibrium ratio of S wave to P wave energies is roughly given by the ratio of the P wave to S wave phase velocities. Although this is merely a precursor of the actual 3D problem with multiple length scales to be investigated, it demonstrates the applicability of the method to address questions of discrimination.

And finally, in chapter 5 we draw some conclusions from our exercises, and discuss work currently in progress, which will utilize the the techniques developed in this report to address more pertinent and realistic problems related to seismic discrimination.

SECTION 2

THE METHOD

2.1 DERIVATION OF THE RECURSION RELATIONS

The phase-screen method may be formulated as an initial value problem. Between any consecutive pair of phase screens the uniform elastodynamic wave equation for the displacement vector, using the average values for the parameters of the medium, is solved. The unique solution in that region is determined by specifying the initial value of the displacement on the first of the two screen. This initial data is obtained by evaluating the displacement in the previous region at this screen and modifying the phase by a position dependent phase factor. The solution in each region may be expressed as a Fourier expansion, decomposed into S and P waves. The Fourier coefficients of the successive solution may be determined in terms of the Fourier coefficients of the previous solution and the phase factor. Thus by knowing the initial displacement produced by a source, the displacement after N phase screens may be recursively determined.

The elastic wave equation for the displacement vector in a uniform medium, and in the absence of external forces is

$$\rho\frac{\partial^2 u}{\partial t^2} = \mu\nabla^2 u + (\lambda + \mu)\nabla(\nabla \cdot u), \qquad (10)$$

where u is the displacement vector, μ and λ are the average Lamé moduli, and ρ is the average density of the medium. The linearity of this equation allows the solutions to be decomposed into S and P waves. Thus the displacement vector may be expressed as the sum

$$u = u_P + u_S, \qquad (11)$$

where the two pieces are chosen to satisfy the constraints

$$\nabla \times u_P = 0 \qquad (12)$$

9

$$\nabla \cdot \mathbf{u}_S = 0. \tag{13}$$

It may readily be shown that this separation can always be accomplished, and that it is unique. Using this decomposition the wave equation reduces to two simple homogeneous wave equations of the form

$$\frac{1}{c_P^2}\frac{\partial^2 \mathbf{u}_P}{\partial t^2} = \nabla^2 \mathbf{u}_P \tag{14}$$

$$\frac{1}{c_S^2}\frac{\partial^2 \mathbf{u}_S}{\partial t^2} = \nabla^2 \mathbf{u}_S, \tag{15}$$

where c_P and c_S are the mean propagation speeds for the respective disturbances, given in terms of the density and Lamé moduli by

$$c_P = \left(\frac{\lambda + 2\mu}{\rho}\right)^{1/2} \tag{16}$$

$$c_S = \left(\frac{\mu}{\rho}\right)^{1/2}. \tag{17}$$

The general form of the solution of the these equations that propagates in the forward direction is

$$\mathbf{u}(\mathbf{r}, t) = \int dk_x dk_y \left[\hat{e}_P A(k_x, k_y)e^{i\mathbf{k}_P \cdot \mathbf{r}} + \hat{e}_S^\alpha B_\alpha(k_x, k_y)e^{i\mathbf{k}_S \cdot \mathbf{r}}\right]e^{-i\omega t}, \tag{18}$$

where $A(k_x, k_y)$ and $B_\alpha(k_x, k_y)$ are Fourier coefficients for the P wave and the two polarizations of the S wave respectively, and $\mathbf{r} = (x, z)$. There is an implicit sum over α from 1 to 2 in this expression, following the standard convention of summing over repeated indices unless otherwise specified. For simplicity, the factor of $e^{-i\omega t}$ will be suppressed throughout the rest of the analysis since all of the solutions we are interested in here will have the same time dependence. Note that the three dimensional Fourier expansion, which is typically used to express solutions of this type, has been reduced to a double integral by use of the dispersion relations, which allow the wave vectors to be expressed solely in terms of k_x and k_y as

10

$$k_P = (k_z, k_y, (w^2/c_P^2 - k_z^2 - k_y^2)^{1/2}) \tag{19}$$

$$k_S = (k_z, k_y, (w^2/c_S^2 - k_z^2 - k_y^2)^{1/2}). \tag{20}$$

The longitudinal and transverse unit vectors, $\hat{e}_P$ and $\hat{e}_S^\alpha$, are defined such that the constraints of eqs. (12,13) are satisfied, i. e. $k_P \times \hat{e}_P = 0$, and $k_S \cdot \hat{e}_S^\alpha = 0$, $\alpha = 1, 2$. The unit vectors satisfying these constraints are

$$\hat{e}_P = \hat{k}_P = \frac{c_P}{w}(k_z, k_y, k_{Pz}) \tag{21}$$

$$\hat{e}_S^1 = \frac{\hat{j} \times \hat{k}_S}{|\hat{j} \times \hat{k}_S|} = \frac{c_S}{w}(1 - \frac{c_S^2 k_y^2}{w^2})^{-1/2}(k_{Sz}, 0, -k_z) \tag{22}$$

$$\hat{e}_S^2 = \frac{\hat{k}_S \times \hat{e}_S^1}{|\hat{k}_S \times \hat{e}_S^1|} = \frac{c_S^2}{w^2}(1 - \frac{c_S^2 k_y^2}{w^2})^{-1/2}(-k_z k_y, \frac{w^2}{c_S^2} - k_y^2, -k_y k_{Sz}), \tag{23}$$

where k_{Pz} and k_{Sz} are the z-components of eqs. (19,20) respectively.

For a given set of Fourier coefficients, propagation between the phase screens is accomplished using eq. (18). Let us now introduce a phase screen at $z = \Delta z$ to compensate for the previously ignored detailed structure. Schematically, if the initial displacement vector, $u^{(0)}$, is specified, then the resultant displacement vector beyond the screen, denoted by $u^{(1)}$, is

$$u^{(1)}|_{z=\Delta z_+} = u^{(0)}|_{z=\Delta z_-} e^{i\Delta(z,y)}. \tag{24}$$

The superscripts on the u's will be used to indicate the number of phase screens the wave has been propagated through. The solution for any value of the superscript takes on a slightly modified form of the general solution of eq. (18). After N phase screens the displacement vector is

$$\begin{aligned} u^{(N)}(r) &= \int d^2k \left\{ \hat{e}_P A^{(N)}(k_z, k_y) e^{ik_{Pz}(z-N\Delta z)} \right. \\ &\quad \left. + \hat{e}_S^\alpha B_\alpha^{(N)}(k_z, k_y) e^{ik_{Sz}(z-N\Delta z)} \right\} e^{ik_z z + ik_y y}. \end{aligned} \tag{25}$$

11

The Fourier coefficients have been defined with the exponential factors that depend on N already factored out to simplify the initial value equation at $z = N\Delta z$.

At this point we depart from the traditional phase-screen approximation for scalar waves, which has been realized, as in eq. (24), by multiplying the entire wave of the previous region by an overall position dependent (but independent of k_x and k_y) phase to provide the initial data for the solution in the next region. In our approach we will multiply the longitudinal and transverse contributions by different Δ-phases, which depend on the appropriate phase velocity for each.

Furthermore, each Fourier mode is multiplied by its own phase factor, i. e. the Δ-phases depend on k_x and k_y. This simply reflects the fact that the phase the wave accumulates from propagating some distance in the z-direction depends on the angle, relative to the z-axis, at which it propagates. This angle is given by

$$\arctan((k_x^2 + k_y^2)^{1/2}/(w^2/c^2 - k_x^2 - k_y^2)^{1/2}). \qquad (26)$$

For small angle propagation the phase is, however, independent of the angle to first order, and hence independent of k_x and k_y. This is satisfied if $k_x, k_y \ll w/c$, such that $k_z \approx w/c$. This will be true for either scalar or vector waves if the typical length scales, in the plane perpindicular to the z-axis, are much greater than w/c (c represents either the transverse or longitudinal speed for the case of vector waves). We are, however, interested in problems of elastic wave propagation with length scales, frequencies, and speeds that do not strictly satisfy this condition, and hence the phase accumulated is not independent of k_x and k_y.

Incorporating these two extra features, if $A^{(N-1)}(k_x, k_y)$ and $B_a^{(N-1)}(k_x, k_y)$ are the coefficients of the expansion of $u^{(N-1)}$, i. e. the wave having been already propagated through $N-1$ phase screens, then the initial value equation for $u^{(N)}$ may be expressed as

$$u^{(N)}(r)|_{z=N\Delta z_+} = \int d^2k \left\{ \hat{e}_P A^{(N-1)}(k_x, k_y) e^{i\Delta^{(P)}(k_x, k_y, x, y)} \right.$$
$$\left. + \hat{e}_S^a B_a^{(N-1)}(k_x, k_y) e^{i\Delta^{(S)}(k_x, k_y, x, y)} \right\} e^{ik_x x + ik_y y}, \qquad (27)$$

where the uniform phase that was acquired in propagating from $(N-1)\Delta z$ to $N\Delta z$ has been absorbed into the definitions of the Δ-phases.

12

The coefficients $A^{(N)}(k)$ and $B_\alpha^{(N)}(k)$ may be determined in terms of $A^{(N-1)}(k)$ and $B_\alpha^{(N-1)}(k)$ and the Δ-phases by setting the RHS of this equation equal to the RHS of eq. (25), evaluated at $z = N\Delta z$, and then multiplying both sides of this new equation by $e^{-ik_x'x-ik_y'y}$, integrating over x and y from $-\infty$ to $+\infty$, and projecting onto the appropriate polarization vectors defined above. The result of this procedure is

$$
\begin{aligned}
A^{(N)}(k_x, k_y) &= \frac{1}{\hat{k}_S \cdot \hat{k}_P} \int dx\, dy \int d^2k'\; e^{i(k_x'-k_x)x+i(k_y'-k_y)y} \\
&\quad \cdot \left\{ \hat{k}_S \cdot \hat{e}_P(k_x', k_y') A^{(N-1)}(k_x', k_y') e^{i\Delta^{(P)}(k_x',k_y',x,y)} \right. \\
&\quad \left. + \; \hat{k}_S \cdot \hat{e}_S^\alpha(k_x', k_y') B_\alpha^{(N-1)}(k_x', k_y') e^{i\Delta^{(S)}(k_x',k_y',x,y)} \right\}
\end{aligned}
\tag{28}
$$

$$
\begin{aligned}
B_\alpha^{(N)}(k_x, k_y) &= \frac{1}{\hat{k}_S \cdot \hat{k}_P} \int dx\, dy \int d^2k'\; e^{i(k_x'-k_x)x+i(k_y'-k_y)y} \left(\hat{k}_S \times \hat{e}_S^\alpha(k_x', k_y') \right) \cdot \\
&\quad \cdot \left\{ \left(\hat{k}_P \times \hat{e}_P(k_x', k_y') \right) A^{(N-1)}(k_x', k_y') e^{i\Delta^{(P)}(k_x',k_y',x,y)} \right. \\
&\quad \left. + \; \left(\hat{k}_P \times \hat{e}_S^\beta(k_x', k_y') \right) B_\beta^{(N-1)}(k_x', k_y') e^{i\Delta^{(S)}(k_x',k_y',x,y)} \right\},
\end{aligned}
\tag{29}
$$

where the vector products may be determined from eqs. (19-23).

As a quick check that the results of eqs. (28,29) are sensible, note that if the Δ-phases are independent of x and y, then the $x - y$ integration may be performed to yield a product of delta functions of $k_x' - k_x$ and $k_y' - k_y$. The integral over d^2k' may also be performed now, replacing k' everywhere with k. Evaluating the vector products, it becomes clear that the contribution to $A^{(N)}$ involves only $A^{(N-1)}$, and not $B_\alpha^{(N-1)}$. The analogous result is true for each of the $B_\alpha^{(N)}$ as well. This shows that if the medium is truly uniform, there is no interconversion between the P and two types of S waves. However, if the Δ-phases do depend on the $x - y$ coordinates, as they will for interesting problems, the coefficients of the P wave after the Nth phase screen depends on both polarizations of the S wave and the P wave of the preceding region; a similar result is true for the S waves as well. Thus the Δ-phases encode information about the scattering and wave type conversion as the wave propagates through an inhomogeneous medium.

13

The Δ-phases at the Nth phase screen in terms of the velocity anomalies between $(N-1)\Delta z$ and $N\Delta z$ are

$$\Delta^{(P)}(k_z, k_y, x, y) = \int_{(N-1)\Delta z}^{N\Delta z} dz' \left[\left(\frac{w}{c_P + \delta c_P(x, y, z')} \right)^2 - k_z^2 - k_y^2 \right]^{1/2}, \qquad (30)$$

and a similar expression with P→ S. At this point the phase-screen method has been reduced to finding expressions for $\delta c_P(x, y, z')$ and $\delta c_S(x, y, z')$ for the physical problem, and specifying the initial form of the wave. In the next chapter we will look at a particular example where their spatial distribution is given deterministically from the medium. Eventually, however, they will be treated as stochastic quantities. First, however, there are some further general results to be obtained.

2.2 MARGINAL NUMBER OF PHASE SCREENS

To determine the number of phase screens to be used, a self-contained method is needed. In the next chapter we will have an exact solution with which to compare. We could increase the number of phase screens per observation distance until the two solutions agree as well as they will. For most problems, however, the exact solution is not accessible. We will determine the marginal number of phase screens needed (MNPS for short) such that the phase-screen solution converges to its asymptotic answer to within some given tolerance as the number of phase screens are increased. This is self-contained and will optimize computer time, using only the necessary number of phase screens that yields an answer close to the the asymptotic answer one would obtain if there were an infinite number of phase screens.

More explicitly, to determine the MNPS, a Cauchy criterion of sorts is used. The distributions of velocity anomalies are chosen, and then the phase-screen answer is computed, adding more and more phase screens for a fixed observation distance. The MNPS is determined when the norm squared of the difference between successive displacement vectors, one computed with K more phase screens than the other, averaged over x and y, converges to within a specified tolerance.

For convenience, we write the displacement vector as

$$u^{(M)}(r) = \int d^2k \left\{ \hat{i} u_z^{(M)}(k_z, k_y, z) + \hat{j} u_y^{(M)}(k_z, k_y, z) + \hat{k} u_z^{(M)}(k_z, k_y, z) \right\} e^{ik_z x + ik_y y},$$
$$(31)$$

14

where the superscript M in this expression denotes the total number of phase screens used for a given observation distance. The norm squared of the difference of two displacement vectors, both the same except that one is calculated using K more phase screens than the other, is

$$
\begin{aligned}
\|u^{(M)} - u^{(M-K)}\|^2 &= \left\| \int d^2k \left\{ \hat{\imath} \left(u_z^{(M)}(k) - u_z^{(M-K)}(k) \right) \right.\right. \\
&\quad + \left. \hat{\jmath} \left(u_y^{(M)}(k) - u_y^{(M-K)}(k) \right) + \hat{k} \left(u_z^{(M)}(k) - u_z^{(M-K)}(k) \right) \right\} e^{ik_x x + ik_y y} \Big\|^2 \\
&= \int d^2k\, d^2k' \left\{ \left(u_z^{(M)}(k) - u_z^{(M-K)}(k) \right) \left(u_z^{(M)}(k')^* - u_z^{(M-K)}(k')^* \right) \right. \\
&\quad + \left(u_y^{(M)}(k) - u_y^{(M-K)}(k) \right) \left(u_y^{(M)}(k')^* - u_y^{(M-K)}(k')^* \right) \\
&\quad + \left. \left(u_z^{(M)}(k) - u_z^{(M-K)}(k) \right) \left(u_z^{(M)}(k')^* - u_z^{(M-K)}(k')^* \right) \right\} e^{i(k_x - k_x')x + i(k_y - k_y')y}.
\end{aligned}
$$

$$(32)$$

Integrating this quantity over x and y, and dividing by the length of the interval in each direction, yields a product of delta functions of the wave numbers as the lengths of the intervals go to infinity. The average of the norm of the squared difference, denoted $ANSD$, is given by

$$
\begin{aligned}
ANSD(z_f) &= \left(\frac{1}{2L} \right)^2 \int_{-L}^{L} dx \int_{-L}^{L} dy\, \|u^{(M)}(x,y,z_f) - u^{(M-K)}(x,y,z_f)\|^2 \\
&= \int d^2k \left\{ |u_z^{(M)}(k,z_f) - u_z^{(M-K)}(k,z_f)|^2 \right. \\
&\quad + \left. |u_y^{(M)}(k,z_f) - u_y^{(M-K)}(k,z_f)|^2 + |u_z^{(M)}(k,z_f) - u_z^{(M-K)}(k,z_f)|^2 \right\} \\
&\leq tolerance.
\end{aligned}
$$

$$(33)$$

The smallest value of M such that this criterion is satisfied will determine the number of phase screens to be used.

15

2.3 ENERGY FLUX

To conclude the general results, we compute an expression for the time-averaged energy flux for both the longitudinal and transverse displacements in terms of the Fourier coefficients of the phase-screen method. The energy flux will also be averaged over the $x - y$ plane, which allows the total energy to be expressed as the sum of the individual energies of the P and the two components of S waves. Thus as a function of z, the ratios of P to S and S_H to S_V (the two polarization of the S wave) may be simply determined. Also, the ratio of transmitted to incident fluxes may be extremized with respect to the parameters of the medium, providing a means to determine what types of regions produce significant or small wave type conversion.

The energy flux given in terms of the displacement is

$$S_i = -\lambda \left(\nabla \cdot \mathbf{u}\right) \frac{\partial u_i}{\partial t} - \mu \sum_j \left(\frac{\partial u_i}{\partial z_j} + \frac{\partial u_j}{\partial z_i}\right) \frac{\partial u_j}{\partial t}, \tag{34}$$

where u in this expression represents only the real part of the complex displacement, and the subscripts refer to the cartesian components. Time-averaging this expression produces

$$\overline{S}_i = \frac{1}{2} Re \left\{ -\lambda \left(\nabla \cdot \mathbf{u}\right) (i\omega u_i^*) - \mu \sum_j \left(\frac{\partial u_i}{\partial z_j} + \frac{\partial u_j}{\partial z_i}\right) (i\omega u_j^*) \right\}, \tag{35}$$

where now u represents the full complex displacement without the time-dependent exponential phase.

Inserting the displacement, given by eq. (25), into this expression, and averaging over the $x - y$ plane, the only nonvanishing component of the averaged fluxes are the z-components, which for the Nth region may be expressed as

$$\overline{S}_{P,z}^{(N)} = \frac{1}{2}\rho\omega^2 c_P \int_{|k|< \frac{\omega}{c_P}} d^2k \left(1 - \frac{c_P^2 |k|^2}{\omega^2}\right)^{1/2} \left|A^{(N)}(k_z, k_y)\right|^2 \tag{36}$$

$$\overline{S}_{S\alpha,z}^{(N)} = \frac{1}{2}\rho\omega^2 c_S \int_{|k|< \frac{\omega}{c_S}} d^2k \left(1 - \frac{c_S^2 |k|^2}{\omega^2}\right)^{1/2} \left|B_\alpha^{(N)}(k_z, k_y)\right|^2. \tag{37}$$

16

where $\alpha = 1, 2$ and $|k| = \sqrt{k_x^2 + k_y^2}$. The limits of integration are due to the fact that for larger $|k|$ the modes are evanescent, and do not contribute a real part to the flux, as should be expected for a non-dissipative medium. From these expressions it is obvious that energy is conserved throughout the region between any consecutive pair of phase screens. Energy conservation from one region to the next is not nearly so trivial, and will now be examined.

2.4 MATRIX FORMULATION AND ENERGY CONSERVATION

The examination of energy conservation is most efficiently performed using a matrix representation of the recursion relations. Although there exists a analogous matrix representation in three dimensions, and a generalization for continuous values of the wave number, for the purposes of the rest of this report, and to clarify the details, we shall consider two dimensional media with periodic boundary conditions in the x-direction. The 2D problem may be recovered as a special case of the 3D problem by setting $k_y = 0$, and the periodic boundary conditions replace the continuous variable k_x with $m\pi/2d$, where the period is $4d$ and m is an integer; the corresponding integrals are replaced with sums. The Fourier coefficients B_{1m} decouple from A_m and B_{1m} in the recursion relations when $k_y = 0$, and hence will be set to zero.

Dropping the '1' subscript from B_{1m}, we shall rescale the Fourier coefficients as

$$A_m^{(N)} \longrightarrow \left(c_P \left(1 - \left(\frac{m\pi c_P}{2dw} \right)^2 \right)^{1/2} \right)^{-1/2} A_m^{(N)} \tag{38}$$

$$B_m^{(N)} \longrightarrow \left(c_S \left(1 - \left(\frac{m\pi c_S}{2dw} \right)^2 \right)^{1/2} \right)^{-1/2} B_m^{(N)}. \tag{39}$$

and define the vector of Fourier coefficients

$$|V^{(N)}\rangle = \left(A_{-M_P}^{(N)}, ..., A_{-1}^{(N)}, A_0^{(N)}, A_1^{(N)}, ..., A_{M_P}^{(N)}, B_{-M_S}^{(N)}, ..., B_{-1}^{(N)}, B_0^{(N)}, B_1^{(N)}, ..., B_{M_S}^{(N)} \right)^T \tag{40}$$

where M_P and M_S are the greatest integers less than $2dw/\pi c_P$ and $2dw/\pi c_S$ respectively, and T denotes the transpose of the row vector. Only the modes with harmonic

17

s-dependence are included in this vector. For integers larger than these values the modes are evanescent, and will not be inclu'ied. This vector may be written schematically in block form as

$$|V^{(N)}\rangle = \begin{pmatrix} A_m^{(N)} \\ B_\mu^{(N)} \end{pmatrix}, \qquad (41)$$

and the matrix that represents the recursion relations may also be expressed in block form as

$$U = \begin{pmatrix} U_{mn}^{PP} & U_{m\nu}^{PS} \\ U_{\mu n}^{SP} & U_{\mu\nu}^{SS} \end{pmatrix}, \qquad (42)$$

where the integers m, n range from $-M_P$ to $+M_P$, and the integers μ, ν range from $-M_S$ to $+M_S$. The off-diagonal blocks represent conversion of one type of wave into another; their explicit form will be determined shortly. The recursion relations for the Fourier coefficients may now be expressed as

$$\begin{pmatrix} A_m^{(N)} \\ B_\mu^{(N)} \end{pmatrix} = \begin{pmatrix} U_{mn}^{PP} & U_{m\nu}^{PS} \\ U_{\mu n}^{SP} & U_{\mu\nu}^{SS} \end{pmatrix} \begin{pmatrix} A_n^{(N-1)} \\ B_\nu^{(N-1)} \end{pmatrix}, \qquad (43)$$

where the summation convention is employed, or equivalently as

$$|V^{(N)}\rangle = U|V^{(N-1)}\rangle. \qquad (44)$$

In addition to setting $k_y = 0$ and making k_z discrete, the Δ-phases may be expanded in Fourier series as

$$e^{i\Delta_m^{(P)}(s)} = \sum_a D_{ma}^{(P)} e^{ia\pi s/2d}. \qquad (45)$$

and a similar expression for the S wave Δ-phase. Combining this information with eqs. (28,29) yields

18

$$U_{m,n}^{PP} = \left(\frac{1-\left(\frac{m\pi c_P}{2d_P}\right)^2}{1-\left(\frac{n\pi c_P}{2d\omega}\right)^2}\right)^{1/4} \frac{\left(1-\left(\frac{m\pi c_S}{2d\omega}\right)^2\right)^{1/2}\left(1-\left(\frac{n\pi c_P}{2d\omega}\right)^2\right)^{1/2}+\left(\frac{m\pi c_S}{2d\omega}\right)\left(\frac{n\pi c_P}{2d\omega}\right)}{\left(1-\left(\frac{m\pi c_P}{2d\omega}\right)^2\right)^{1/2}\left(1-\left(\frac{n\pi c_S}{2d\omega}\right)^2\right)^{1/2}+\left(\frac{m\pi c_P}{2d\omega}\right)\left(\frac{n\pi c_S}{2d\omega}\right)} D_{n,m-n}^{(P)} \qquad (46)$$

$$U_{m,\nu}^{PS} = \sqrt{\frac{c_P}{c_S}}\left(\frac{1-\left(\frac{m\pi c_P}{2d\omega}\right)^2}{1-\left(\frac{\nu\pi c_S}{2d\omega}\right)^2}\right)^{1/4} \frac{\left(\frac{m\pi c_P}{2d\omega}\right)\left(1-\left(\frac{\nu\pi c_S}{2d\omega}\right)^2\right)^{1/2}-\left(\frac{\nu\pi c_S}{2d\omega}\right)\left(1-\left(\frac{m\pi c_S}{2d\omega}\right)^2\right)^{1/2}}{\left(1-\left(\frac{m\pi c_P}{2d\omega}\right)^2\right)^{1/2}\left(1-\left(\frac{\nu\pi c_S}{2d\omega}\right)^2\right)^{1/2}+\left(\frac{m\pi c_P}{2d\omega}\right)\left(\frac{\nu\pi c_S}{2d\omega}\right)} D_{\nu,m-\nu}^{(S)} \qquad (47)$$

$$U_{\mu,n}^{SP} = \sqrt{\frac{c_S}{c_P}}\left(\frac{1-\left(\frac{\mu\pi c_S}{2d\omega}\right)^2}{1-\left(\frac{n\pi c_P}{2d\omega}\right)^2}\right)^{1/4} \frac{\left(\frac{n\pi c_P}{2d\omega}\right)\left(1-\left(\frac{\mu\pi c_P}{2d\omega}\right)^2\right)^{1/2}-\left(\frac{\mu\pi c_S}{2d\omega}\right)\left(1-\left(\frac{n\pi c_P}{2d\omega}\right)^2\right)^{1/2}}{\left(1-\left(\frac{\mu\pi c_P}{2d\omega}\right)^2\right)^{1/2}\left(1-\left(\frac{n\pi c_S}{2d\omega}\right)^2\right)^{1/2}+\left(\frac{\mu\pi c_S}{2d\omega}\right)\left(\frac{n\pi c_S}{2d\omega}\right)} D_{n,\mu-n}^{(P)} \qquad (48)$$

$$U_{\mu,\nu}^{SS} = \left(\frac{1-\left(\frac{\mu\pi c_S}{2d\omega}\right)^2}{1-\left(\frac{\nu\pi c_S}{2d\omega}\right)^2}\right)^{1/4} \frac{\left(1-\left(\frac{\mu\pi c_P}{2d\omega}\right)^2\right)^{1/2}\left(1-\left(\frac{\nu\pi c_S}{2d\omega}\right)^2\right)^{1/2}+\left(\frac{\mu\pi c_P}{2d\omega}\right)\left(\frac{\nu\pi c_S}{2d\omega}\right)}{\left(1-\left(\frac{\mu\pi c_P}{2d\omega}\right)^2\right)^{1/2}\left(1-\left(\frac{\mu\pi c_S}{2d\omega}\right)^2\right)^{1/2}+\left(\frac{\mu\pi c_P}{2d\omega}\right)\left(\frac{\mu\pi c_S}{2d\omega}\right)} D_{\nu,\mu-\nu}^{(S)}. \qquad (49)$$

The total energy flux in the Nth region, averaged over time and the x-coordinate, is

$$\bar{S}_z^{(N)} = \frac{1}{2}\rho\omega^2\langle V^{(N)}|V^{(N)}\rangle. \qquad (50)$$

This simple form was made possible by the rescalings of the Fourier coefficients in eqs. (38,39). The energy of the P wave is given by the first $2M_P + 1$ terms of this expression, and the energy of the S wave is given by the remaining terms. Using the recursion relations this may be re-expressed as

$$\bar{S}_z^{(N)} = \frac{1}{2}\rho\omega^2\langle V^{(N-1)}|U^\dagger U|V^{(N-1)}\rangle. \qquad (51)$$

Thus for energy to be conserved from one region to the next the recursion matrix U must be unitary, i. e. if I is defined to be the identity matrix, then

$$U^\dagger U = UU^\dagger = I. \qquad (52)$$

19

For general Δ-phases the recursion matrix is not unitary, although for the range of parameters for which the phase-screen method is expected to be valid, it is almost unitary. Almost unitary is defined to mean that the eigenvalues of the matrix are close to being unimodular, and the commutator of the matrix with its adjoint has small entries. Although the violation of energy conservation at each phase screen may be less than a tenth of a percent, the cumulative energy violation after propagating through a thousand phase screens may be significant. To remedy this problem we have employed the following algorithm.

First, the complex vector $|V\rangle$ is written as a real vector of twice its original length simply by entering the real and imaginary part of each complex entry as pairs of entries in the real vector. The complex matrix U is also put in real form by replacing each complex entry U_{ij} with the 2×2 block

$$\begin{pmatrix} ReU_{ij} & -ImU_{ij} \\ ImU_{ij} & ReU_{ij} \end{pmatrix} \tag{53}$$

If the real matrix corresponding to U is denoted by R, the condition for energy to be conserved is that R be an orthogonal matrix, defined to satisfy

$$R^T R = RR^T = I. \tag{54}$$

The second step of the algorithm is to perform a singular value decomposition of R, *i. e.* write

$$R = O_1 D O_2 \tag{55}$$

where O_1 and O_2 are orthogonal matrices, and D is a diagonal matrix whose entries are the singular values of R. The singular values of a matrix are the positive square roots of the eigenvalues of $R^T R$. This decomposition must be performed by a numerical routine in practice. The matrix R can be said to be almost orthogonal if its singular values are all close to unity. To make R exactly orthogonal we simply replace D with the identity matrix I. Thus

$$R \longrightarrow O_1 O_2, \tag{56}$$

20

which is clearly orthogonal since O_1 and O_2 are both orthogonal.

At this point we have the necessary machinery to work on specific problems, which is what we will turn to now.

SECTION 3

COMPARISON WITH AN EXACT SOLUTION

We shall illustrate the phase-screen method for a problem whose exact solution is tractable without being trivial. The test problem we have chosen, shown in figure 3, is to solve for the elastic displacement vector in a two dimensional medium constructed from two different homogeneous strips of equal width, repeating alternately and infinitely in the x-direction, and of infinite extent in the z-direction, taken to be the forward direction of wave propagation. We shall center the origin at the mid-point of region one, and by convention let the regions both be a distance $2d$ wide.

The exact solution for this problem is calculated first, and then the phase-screen approximation is computed and compared to it. We shall use this comparison to quantitatively understand the limitations of the method. In particular, we examine the limits of the region widths, the magnitudes of velocity fluctuations about the mean, and the propagation distances for which the approximation is valid. We also provide some explanation for why these limits exist. This analysis will yield some guidelines for the range of parameters over which the phase-screen method may be trusted for problems whose exact solutions are not accessible.

Also, the ratio of the flux for a transmitted S wave to the flux of an incident P wave is extremized, for a single phase screen, with respect to the ratio of the width of the regions to the free space wavelength. This analysis is performed for various ratios of c_P/c_S. The same result is computed for an incident S wave and transmitted P wave. This result yields insight into the wavelengths, or equivalently structure sizes, that contribute the most to wave type conversion, and the dependence on the wave speeds.

3.1 THE EXACT SOLUTION

We begin by presenting the exact solution to the problem stated above. By "exact" we mean that there is no fundamental approximation made for the wave equation or the boundary conditions used to solve this problem. Some numerical work must be performed, however, to obtain the final result, which cannot be written in closed form, but the solution may be determined to any desired accuracy.
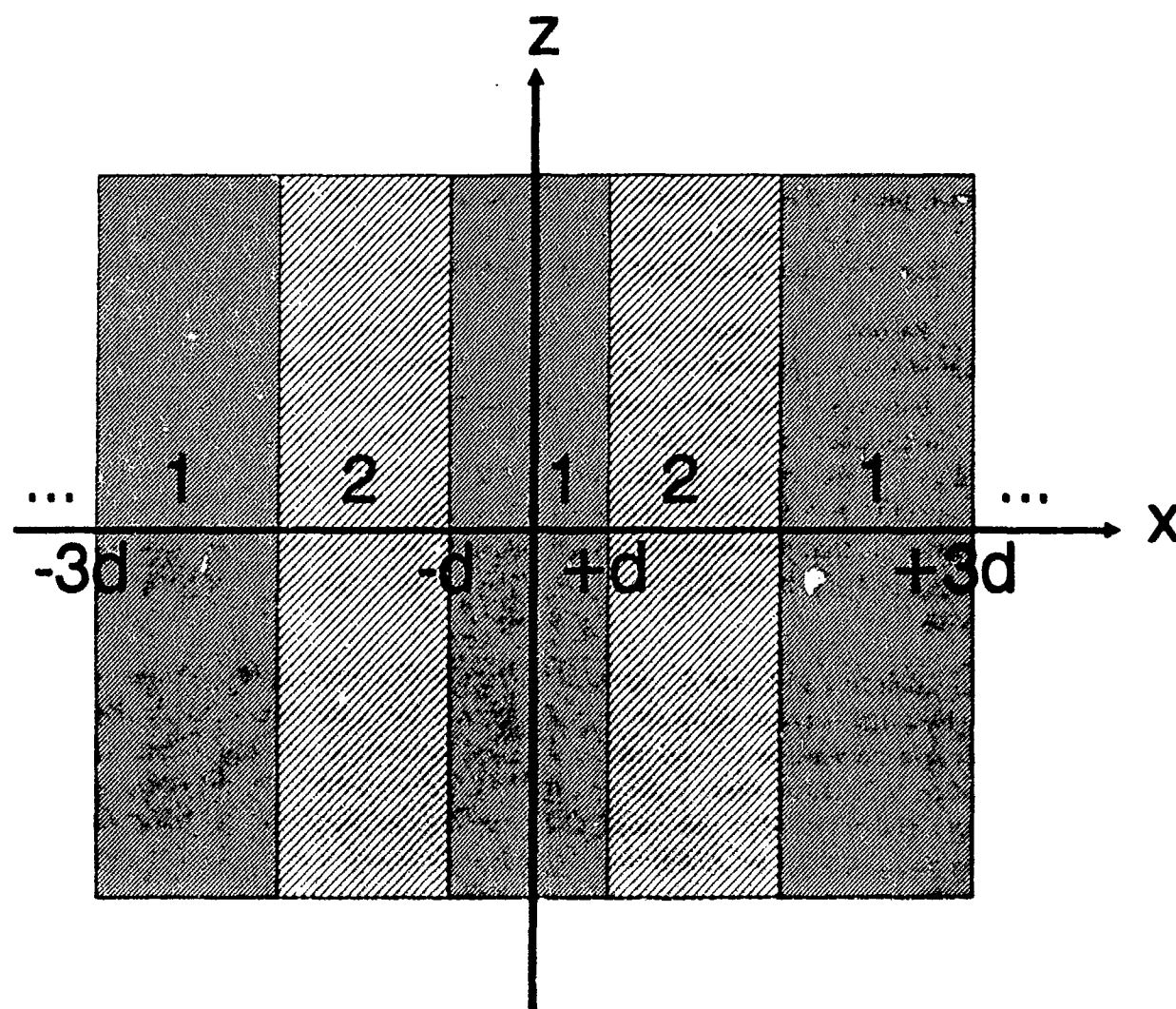
22

Figure 3.   The 2D medium for the test problem is comprised of two alternating homogeneous strips.

The procedure for solving this problem is relatively straightforward. First, the homogeneous wave equation is solved in each region. Then these solutions are matched together, determining the unique solution, by satisfying the boundary conditions at the interfaces and the initial condition for the wave at $z = 0$.

To simplify finding the solution, the symmetries of the problem may be exploited. First, the medium possesses periodic translation invariance in the x-direction. Any pair of neighboring regions, labelled one and two, are indistinguishable from all other such pairs. Only the solution in a fundamental pair of regions must be calculated; the boundary conditions are matched only at the interface between these two regions. The solutions in all other pairs of regions are identical to this one.

Second, the medium is clearly invariant under reflections about the z-axis. Solutions may be separated into parity eigenfunctions that are either even or odd as $x \to -x$. If even and odd parity solutions exist and may be treated separately in each region, the number of unknowns to solve for in the boundary value equations will be reduced by a factor of two. Clearly the solution in the region centered on the z-axis, from $x = -d$ to $x = d$, may be separated into even and odd parity eigenfunctions. We shall now argue that the solution in all of the other regions must be of the same parity, when expanded about the midpoint of that particular region, as the one centered on the z-axis.

Refering to figure 3, parity about the z-axis alone only guarantees, for example, that the solution between $x = d$ and $x = 3d$ is an even or odd reflection of the solution between $x = -3d$ and $x = -d$. However, if we simultaneously invoke translation invariance, there is also parity invariance about all of the lines parallel to the z-axis and centered at the midpoint of each region. Furthermore, the parity of the solution about these lines must be the same, either even or odd, in all of the regions, for the solutions to match smoothly at the interfaces.

To see that these statements are true we argue that the converse results leads to contradictions. Suppose the solutions in the regions from $x = d$ to $x = 3d$ and from $x = -3d$ to $x = -d$ respect the parity symmetry about the z-axis, but not about the lines centered at the midpoints of the two regions. It is trivial to see that these solutions cannot be identical. This contradicts the asumption that there is translation invariance. Pushing this argument slightly further, suppose the solution in the region from $x = -d$ to $x = d$ has a particular parity about the z-axis, and the solution in the region from $x = d$ to $x = 3d$ has the opposite parity about its midpoint. The solution in the region from $x = -3d$ to $x = -d$ that is identical to the solution in the region from $x = d$ to $x = 3d$ cannot join smoothly to the solution in region one at $x = -d$, i. e. the derivative of the displacement with respect to x will

be discontinuous there. Thus the boundary condition involving such derivatives will not be satisfied, and hence this is not a valid solution. These arguments are trivially extended to the other regions as well.

Combining these symmetries, we may arbitrarily choose the fundamental pair of regions to be the one between $x = -d$ and $x = 3d$; the solutions in these two regions may be separated, both into either even or odd eigenfunctions, expanded about the midpoint of that region. For example, the x-dependence of the solution between $x = d$ and $x = 3d$ may be expressed in terms of either even or odd functions of the argument $(x - 2d)$. The boundary conditions at the interface of these two regions have thus been greatly simplified.

The wave equation to solve is the same as eq. (10) except that here there are two regions, each with their own densities, elastic moduli, and hence wave velocities. In each region the general solution corresponds to that of a homogeneous displacement wave. The general solution in region one may be expressed as

$$u_1(r) = \int dk_s \left[\hat{e}_{P_1} A_1(k_s) e^{ik_{P_1} \cdot r} + \hat{e}_{S_1} B_1(k_s) e^{ik_{S_1} \cdot r} \right], \tag{57}$$

and to obtain the solution in region two simply let $1 \to 2$ and $x \to (x - 2d)$.

To solve for the coefficients of the expansion it is necessary to match the boundary conditions at the interface. It is worth noting that we have written the expression above in terms of k_s instead of k_s as for the phase-screen case to simplify matching the boundary conditions for all values of z. Using the dispersion relations, the wave vectors in each region may be written in terms of k_s as

$$k_{P_i} = ((w^2/c_{P_i}^2 - k_s^2)^{1/2}, k_s) \tag{58}$$

$$k_{S_i} = ((w^2/c_{S_i}^2 - k_s^2)^{1/2}, k_s). \tag{59}$$

As discussed, the solutions may be separated by their parity. Note that in order to satisfy the constraints of eqs. (12, 13), if the x-component of the displacement vector has a particular parity, the z-component must have the opposite. Thus there are only two parity eigenfunctions that the solution may decomposed into, which for the sake of convenience will be labelled (even,odd) or (odd,even) according to whether the x-component has even or odd parity respectively. Note also that the initial condition chosen must be consistent with the parity of the solution, e. g. if the incoming wave

25

is a uniform plane P wave, the solution should have even parity for the z-component, and if the incoming wave is a uniform plane S wave, the solution should have even parity for the x-component. We will examine the latter case first. For simplicity, the following definitions will be used:

$$a_i = \left(1 - \frac{c_{P_i}^2 k^2}{w^2}\right)^{1/2} \tag{60}$$

$$b_i = \frac{c_{S_i} k}{w} \tag{61}$$

$$c_i = \frac{c_{P_i} k}{w} \tag{62}$$

$$d_i = \left(1 - \frac{c_{S_i}^2 k^2}{w^2}\right)^{1/2}, \tag{63}$$

where the subscript refers to region one or two. Using these definitions the solution in region one with (even,odd) parity may be written as

$$
\begin{aligned}
u_1(r) \;=\; \int dk &\Big\{\Big[\hat{\imath} a_1 \cos\left(w a_1 x / c_{P_i}\right) + \hat{k} c_1 i \sin\left(w a_1 x / c_{P_i}\right)\Big] A_1(k) \\
&+ \Big[\hat{\imath} b_1 \cos\left(w d_1 x / c_{S_i}\right) - \hat{k} d_1 i \sin\left(w d_1 x / c_{S_i}\right)\Big] B_1(k) \Big\} e^{ikz}. \tag{64}
\end{aligned}
$$

There is a similar expression in region two with $1 \rightarrow 2$ and $x \rightarrow (x - 2d)$. All of the square roots denote the principal value of the complex square root, and $k \geq 0$ since only the forward wave is included.

Now we will proceed to determine the unknown coefficients by solving the boundary conditions at $x = d$. There are two vector boundary conditions at the interface to be satisfied. First, the displacement must be continuous at the interface to insure that the velocities are finite everywhere. And second, the traction (the normal projections of the stress tensor) must be continuous there as well to avoid infinite accelerations.

Continuity of displacement, $u_1(d_-) = u_2(d_+)$, yields the following two equations:

26

$$a_1 \cos\left(wa_1d/c_{P_1}\right) A_1(k) + b_1 \cos\left(wd_1d/c_{S_1}\right) B_1(k) =$$

$$a_2 \cos\left(wa_2d/c_{P_2}\right) A_2(k) + b_2 \cos\left(wd_2d/c_{S_2}\right) B_2(k) \tag{65}$$

$$c_1 \sin\left(wa_1d/c_{P_1}\right) A_1(k) - d_1 \sin\left(wd_1d/c_{S_1}\right) B_1(k) =$$

$$- c_2 \sin\left(wa_2d/c_{P_2}\right) A_2(k) + d_2 \sin\left(wd_2d/c_{S_2}\right) B_2(k). \tag{66}$$

Similarly, continuity of traction at $x = d$, $T_1^{i1}(d_-) = T_2^{i1}(d_+)$, yields two equations. First, the normal projection of the stress tensor may be written in terms of the displacement as

$$T^{i1} = -\lambda \delta^{i1} \nabla \cdot \mathbf{u} - \mu \left(\frac{\partial u^i}{\partial x} + \frac{\partial u^1}{\partial x^i} \right). \tag{67}$$

To clarify the notation, all superscripts here refer to cartesian components of tensors or vectors, and $x^1 = x$, $x^2 = z$. The subscripts, as for the displacement vector, will refer to the particular region. Using the expression for the displacement, eq. (64), the two traction equations are

$$\mu_1 \left\{ \frac{2}{c_{P_1}} a_1 c_1 \cos(wa_1d/c_{P_1})A_1(k) + \frac{1}{c_{S_1}}(b_1^2 - d_1^2)\cos(wd_1d/c_{S_1})B_1(k) \right\} =$$
$$\mu_2 \left\{ \frac{2}{c_{P_2}} a_2 c_2 \cos(wa_2d/c_{P_2})A_2(k) + \frac{1}{c_{S_2}}(b_2^2 - d_2^2)\cos(wd_2d/c_{S_2})B_2(k) \right\} \tag{68}$$

$$\frac{1}{c_{P_1}}\left[2\mu_1 a_1^2 + \lambda_1\right]\sin(wa_1d/c_{P_1})A_1(k) + \frac{2}{c_{S_1}}\mu_1 d_1 b_1 \sin(wd_1d/c_{S_1})B_1(k) =$$
$$- \frac{1}{c_{P_2}}\left[2\mu_2 a_2^2 + \lambda_2\right]\sin(wa_2d/c_{P_2})A_2(k) - \frac{2}{c_{S_2}}\mu_2 d_2 b_2 \sin(wd_2d/c_{S_2})B_2(k). \tag{69}$$

There are four sets of unknown Fourier coefficients, and one set of discrete wave numbers to solve for. We will divide the four boundary condition equations arbitrarily by $B_2(k)$, use three of the equations to solve for A_1/B_2, B_1/B_2, and A_2/B_2,

27

and then insert these expressions into the fourth equation to determine the discrete eigenvalues allowed for k, labelled k_m, where m is an integer. The remaining set of discrete coefficients, $\{B_{2m}\} \equiv \{B_2(k_m)\}$, specifies the shape and overall normalization of the displacement wave, which is given by an initial condition that we will choose at $z = 0$.

As will be shown shortly, the eigenvalue equation is a transcendental equation, making it necessary to solve for the eigenvalues numerically. This forces us to choose specific values for the parameters of the problem. A choice that simplifies the algebra considerably is to let $\lambda_1 = \lambda_2 = 0$ and $\mu_1 = \mu_2$. The densities of the two regions must be different to have an interesting problem, but by making this choice for the elastic moduli, their explicit dependence cancels out of the transcendental equations, and only the phase velocities need to be given numerical values.

The four equations are divided by B_2, however, the solutions of the first three equations for A_1/B_2, B_1/B_2, and A_2/B_2 are all divided by the determinant of the matrix of Cramer's rule when solving a linear system of equations. We will absorb this determinant into the definition of $B_2(k)$, and drop the subscript so that we may write the solution in a symmetric form for the two regions. Using the first three boundary conditions, along with the choices for the Lamé moduli just mentioned, some tedious but straightforward algebra yields the following expressions:

$$\mathcal{L}_1(k) \equiv A_1(k)/B(k) \;=\; c_2(b_2^2 - b_1^2)\sin(wa_2d/c_{P_2})\cos(wd_1d/c_{S_1})\cos(wd_2d/c_{S_2})$$

$$+\;\; a_2b_2d_2\sin(wd_2d/c_{S_2})\cos(wa_2d/c_{P_2})\cos(wd_1d/c_{S_1})$$

$$+\;\; a_2b_1d_1\sin(wd_1d/c_{S_1})\cos(wa_2d/c_{P_2})\cos(wd_2d/c_{S_2}) \quad (70)$$

$$T_1(k) \equiv B_1(k)/B(k) \;=\; a_2b_1c_1\sin(wa_1d/c_{P_1})\cos(wa_2d/c_{l_2})\cos(wd_2d/c_{S_2})$$

$$+\;\; a_1b_1c_2\sin(wa_2d/c_{P_2})\cos(wa_1d/c_{P_1})\cos(wd_2d/c_{S_2}), \quad (71)$$

and similar expressions for $\mathcal{L}_2$ and T_2, but with $1 \leftrightarrow 2$. T_3 is simply the determinant of the matrix discussed above.

Inserting these expressions into the fourth equation, the transcendental eigenvalue equation for k is

$$0 = \tan(wa_2 d/c_{P_2})\tan(wd_1 d/c_{S_1})a_1 b_1 c_1 d_1 + \tan(wa_2 d/c_{P_2})\tan(wd_2 d/c_{S_2})a_1 b_2 c_1 d_2$$

$$+ \tan(wa_1 d/c_{P_1})\tan(wd_1 d/c_{S_1})a_2 b_1 c_2 d_1 + \tan(wa_1 d/c_{P_1})\tan(wd_2 d/c_{S_2})a_2 b_2 c_2 d_2$$

$$+ \tan(wa_1 d/c_{P_1})\tan(wa_2 d/c_{P_2})(b_2^2 - b_1^2)(c_2^2 - c_1^2). \tag{72}$$

It has been written in terms of the tangent function by dividing by the necessary sines and cosines. Writing it in this form simplifies the numerical root finding process because the asymptotes of the tangent functions provide natural limits to search between for the roots. In fact, between any consecutive pair of asymptotes there are either two roots, one root, or no roots.

All that remains to completely specify the solution is to fix the initial shape and normalization of the wave, specified by the set of coefficients $\{B_m\}$. To do this we will choose that at $z = 0$

$$u_1(x,0) = u_2(x,0) = \hat{\imath}. \tag{73}$$

This expression yields four equations, but there is only one set of coefficients $\{B_m\}$. In general, each of these four conditions must be satisfied by a unique linear combination of complete functions. Each linear combination is specified by the set of coefficients that gets multiplied to these complete functions. This implies that unless the functions, that have been used to expand the solution, are equivalent to four complete sets of functions, there is no hope of satisfying the four initial condition equations at $z = 0$; the solution will be over-determined. It is worth noting that the cosine and sine functions used to expand the solution are not orthogonal functions, making it impossible to determine by casual inspection the number of complete sets of functions they comprise. However, an examination of the eigenvalues of k reveals that they may be grouped into pairs. This is much more apparent for the larger values of k. In fact, the discrete pairs asymptotically approach either $in\pi/d$ or $i(n + 1/2)\pi/d$. Combining this with the fact that there are both sine and cosine functions present in the solution indicates that there are actually enough complete sets of functions to satisfy the initial condition. Although this is a only a heuristic argument, we can proceed to actually solve the initial condition to verify that a solution does exist.

Another consequence of the fact that the cosine and sine functions, used to expand the solution, are not orthogonal, is that projecting the solution for the

29

displacement onto the initial condition, as is done in typical Fourier analysis, does not yield the solution for the individual coefficients. Instead we solve for the coefficients numerically using a least squares routine. The variable z is first discretized to the set $\{z_n\}$, and the sum over the discrete values of k_m is truncated. Also, the set $\{B_m\}$ may be written as a column vector of dimension M, where M is the value of m at which the series is truncated. The initial condition may also be written as a column vector of dimension N, where N is four times the number of discrete values of z chosen, since there are two spatial vector components in each of the two regions. The linear transformation that maps the coefficients into the initial condition is an $N \times M$ matrix whose entries depend on k_m and z_n. To solve for the coefficients requires inverting this matrix, which is performed numerically by the least squares routine. To make this clearer, schematically the initial condition at $z = 0$ may be written as

$$
U_n \equiv U(z_n) \equiv \begin{pmatrix} u_{1z} \\ u_{1s} \\ u_{2z} \\ u_{2s} \end{pmatrix}_n = \begin{pmatrix} 1 \\ 0 \\ 1 \\ 0 \end{pmatrix}_n , \tag{74}
$$

where the subscript n labels the discrete values of z. Thus each entry actually represents a column of $N/4$ entries. Also, the general solution at $z = 0$, may be written in the form

$$
U_n = \sum_{m}^{M} M_{nm} B_m . \tag{75}
$$

The solution for the unknown coefficients $\{B_m\}$ is

$$
B_m = \sum_{n}^{N} M_{mn}^{-1} U_n . \tag{76}
$$

Having solved this inversion numerically, and using eqs. (64,70,71), the complete solution for the displacement for $-d < z < d$ with (even,odd) parity is

$$
u_1(r) = \sum_m \left\{ \left[i a_{1m} \cos\left(w a_{1m} z/c_{P_1}\right) + \hat{k} c_{1m} i \sin\left(w a_{1m} z/c_{P_1}\right) \right] \mathcal{L}_{1m} \right.
$$
$$
\left. + \left[i b_{1m} \cos\left(w d_{1m} z/c_{S_1}\right) - \hat{k} d_{1m} i \sin\left(w d_{1m} z/c_{S_1}\right) \right] T_{1m} \right\} B_m e^{ikz} , \tag{77}
$$

30

and the solution for $d < z < 3d$ is the similar except with $1 \rightarrow 2$ and $z \rightarrow (z - 2d)$.

Having calculated the solution above, it is now straightforward to write down the (odd,even) parity solution. In region one, the displacement is

$$\mathbf{u}_1(\mathbf{r}) \;=\; \int dk \left\{ \left[\hat{i} a_1 i \sin\left(w a_1 z / c_{P_1}\right) + \hat{k} c_1 \cos\left(w a_1 z / c_{P_1}\right) \right] A_1(k) \right.$$

$$\left. + \left[\hat{i} b_1 i \sin\left(w d_1 z / c_{S_1}\right) - \hat{k} d_1 \cos\left(w d_1 z / c_{S_1}\right) \right] B_1(k) \right\} e^{ikz}, \qquad (78)$$

and as before, a similar expression for region two with $1 \rightarrow 2$ and $z \rightarrow (z - 2d)$.

Continuity of displacement at $z = d$, $\mathbf{u}_1(d_-) = \mathbf{u}_2(d_+)$, yields the following two equations:

$$a_1 \sin\left(w a_1 d / c_{P_1}\right) A_1(k) + b_1 \sin\left(w d_1 d / c_{S_1}\right) B_1(k) \;=\;$$

$$-\, a_2 \sin\left(w a_2 d / c_{P_2}\right) A_2(k) - b_2 \sin\left(w d_2 d / c_{S_2}\right) B_2(k) \qquad (79)$$

$$c_1 \cos\left(w a_1 d / c_{P_1}\right) A_1(k) - d_1 \cos\left(w d_1 d / c_{S_1}\right) B_1(k) \;=\;$$

$$c_2 \cos\left(w a_2 d / c_{P_2}\right) A_2(k) - d_2 \cos\left(w d_2 d / c_{S_2}\right) B_2(k). \qquad (80)$$

Similarly, continuity of traction at $z = d$, $T_1^{i1}(d_-) = T_2^{i1}(d_+)$, yields

$$\mu_1 \left\{ \frac{2}{c_{P_1}} a_1 c_1 \sin(w a_1 d / c_{P_1}) A_1(k) + \frac{1}{c_{S_1}} (b_1^2 - d_1^2) \sin(w d_1 d / c_{S_1}) B_1(k) \right\} \;=\;$$

$$-\mu_2 \left\{ \frac{2}{c_{P_2}} a_2 c_2 \sin(w a_2 d / c_{P_2}) A_2(k) + \frac{1}{c_{S_2}} (b_2^2 - d_2^2) \sin(w d_2 d / c_{S_2}) B_2(k) \right\} \qquad (81)$$

$$\frac{1}{c_{P_1}} \left[2\mu_1 a_1^2 + \lambda_1 \right] \cos(w a_1 d / c_{P_1}) A_1(k) + \frac{2}{c_{S_1}} \mu_1 d_1 b_1 \cos(w d_1 d / c_{S_1}) B_1(k) \;=\;$$

$$\frac{1}{c_{P_2}} \left[2\mu_2 a_2^2 + \lambda_2 \right] \cos(w a_2 d / c_{P_2}) A_2(k) + \frac{2}{c_{S_2}} \mu_2 d_2 b_2 \cos(w d_2 d / c_{S_2}) B_2(k). \qquad (82)$$

31

As before, using the first three boundary condition equations, choosing $\lambda_1 = \lambda_2 = 0$ and $\mu_1 = \mu_2$, and absorbing the determinant of Cramer's rule into the definition of $B(k)$, the coefficients are

$$\mathcal{L}_1(k) \equiv A_1(k)/B(k) = c_2(b_2^2 - b_1^2)\cos(wa_3d/c_{P_3})\sin(wd_1d/c_{S_1})\sin(wd_2d/c_{S_2})$$

$$+ a_3b_3d_3\cos(wd_3d/c_{S_3})\sin(wa_3d/c_{P_3})\sin(wd_1d/c_{S_1})$$

$$+ a_3b_1d_1\cos(wd_1d/c_{S_1})\sin(wa_2d/c_{P_3})\sin(wd_3d/c_{S_2}) \qquad (83)$$

$$\mathcal{T}_1(k) \equiv B_1(k)/B(k) = a_2b_1c_1\cos(wa_1d/c_{P_1})\sin(wa_2d/c_{P_3})\sin(wd_3d/c_{S_3})$$

$$+ a_1b_1c_2\cos(wa_2d/c_{P_3})\sin(wa_1d/c_{P_1})\sin(wd_3d/c_{S_3}), \qquad (84)$$

and similar expressions for $\mathcal{L}_2$ and $\mathcal{T}_2$, but with $1 \leftrightarrow 2$.

Inserting these expressions into the fourth equation, the transcendental eigenvalue equation for k is

$$0 = \tan(wa_1d/c_{P_1})\tan(wd_2d/c_{S_2})a_1b_1c_1d_1 + \tan(wa_1d/c_{P_1})\tan(wd_1d/c_{S_1})a_1b_2c_1d_2$$

$$+ \tan(wa_3d/c_{P_3})\tan(wd_2d/c_{S_3})a_2b_1c_2d_1 + \tan(wa_2d/c_{P_3})\tan(wd_1d/c_{S_1})a_3b_2c_2d_3$$

$$+ \tan(wd_1d/c_{S_1})\tan(wd_2d/c_{S_2})(b_3^2 - b_1^2)(c_2^2 - c_1^2). \qquad (85)$$

The initial condition at $z = 0$ for the (odd,even) parity case is

$$u_1(z,0) = u_2(z,0) = \hat{k}, \qquad (86)$$

and as before, the coefficients will be solved for using a least squares routine. With these coefficients, the solution may be written as

$$u_1(r) = \sum_m \left\{ \left[ia_{1m} \hat{i} \sin\left(wa_{1m}z/c_{P_1}\right) + \hat{k}c_{1m} \cos\left(wa_{1m}z/c_{P_1}\right) \right] \mathcal{L}_{1m} \right.$$

$$\left. + \left[ib_{1m} \hat{i} \sin\left(wd_{1m}z/c_{S_1}\right) - \hat{k}d_{1m} \cos\left(wd_{1m}z/c_{S_1}\right) \right] \mathcal{T}_{1m} \right\} B_m e^{ikz}. \quad (87)$$

For any other initial condition that is uniform as a function of z, the solution will be a linear combination of the displacement vectors given by eqs. (77,87). For initial conditions that do depend on z, the only change in the solution is that the set of coefficients $\{B_m\}$ must be determined in the same manner as before, but for the new initial condition. This completes the analysis of the exact solution, and we now turn to the phase-screen solution of the same problem.

3.2   THE PHASE SCREEN SOLUTION

Now that the exact solution has been calculated, we would like to compute the phase-screen approximation for the same physical problem, and then compare the two. Figure 4 depicts how the problem will be treated using the phase-screen method. The wave is propagated uniformly between phase screens, as discussed in chapter 2. The phase of the wave at the phase screen is then retarded uniformly for values of z corresponding to region one, and advanced uniformly for values of z corresponding to region two. Because of the periodicity of the problem, the general solution of the uniform wave equation, written as a Fourier integral in chapter 2, may be expressed as a discrete series. Thus the displacement vector between the Nth and the $(N + 1)^{th}$ phase screens may be written as

$$u^{(N)}(r) = \sum_m \left\{ \left(\hat{i}c_m + \hat{k}a_m \right) A_m^{(N)} e^{iwa_m(s-N\Delta s)/c_P} \right.$$

$$\left. + \left(\hat{i}d_m - \hat{k}b_m \right) B_m^{(N)} e^{iwd_m(s-N\Delta s)/c_S} \right\} e^{im\pi z/2d}, \quad (88)$$

where a_m, b_m, c_m, d_m are of the same form as those defined in eqs. (60,61,62,63) except that the k refers to the z-component of the wave vector in this case, given by $k \rightarrow m\pi/2d$, and instead of carrying a subscript that depends on the wave velocities of the two regions, there is only one quantity of each type that depends on the average of either the tranverse or longitudinal velocities of the two regions.

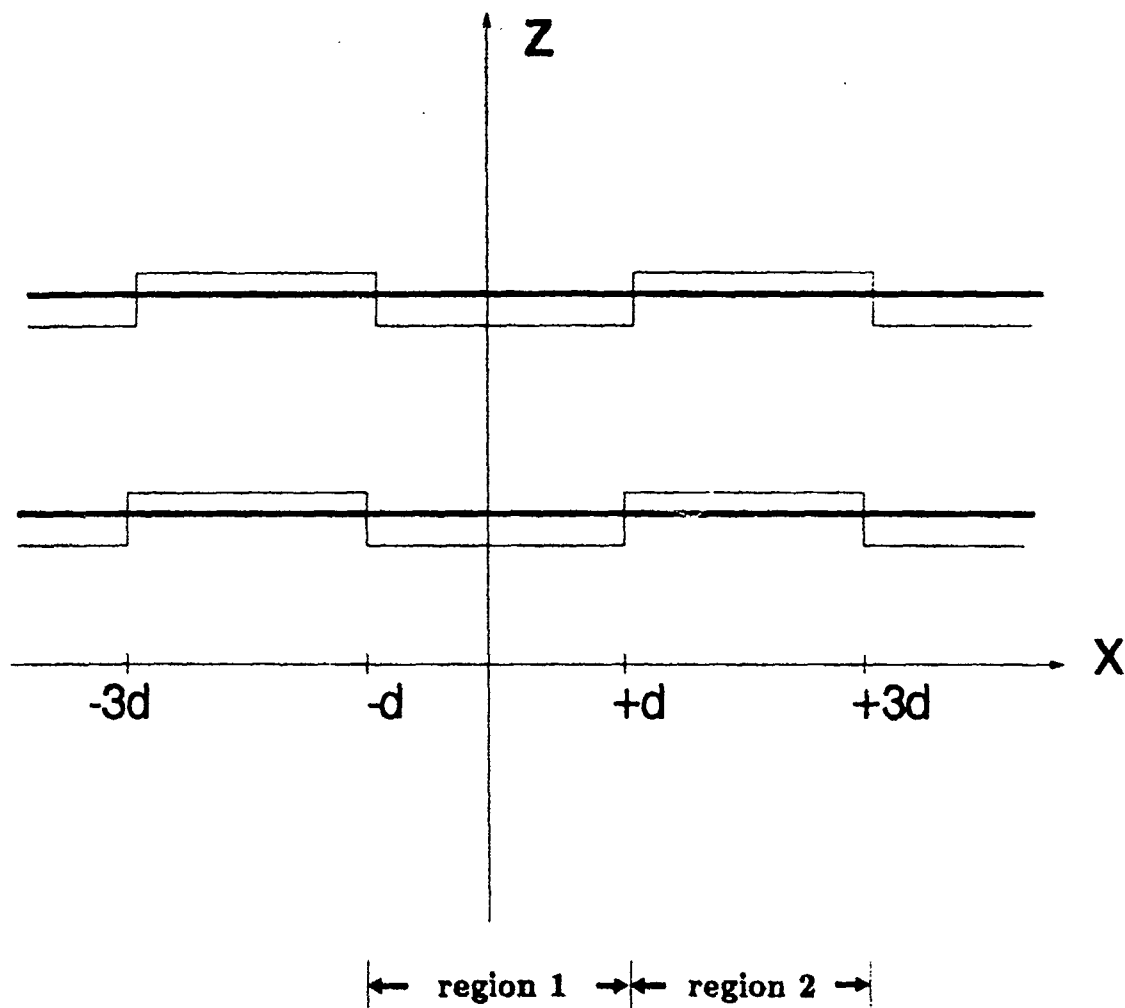At this point the velocity anomalies need to be specified for the problem. For the P wave in region one

Figure 4. The phase-screen treatment of the test problem introduces the phase screens, represented by the heavy solid lines. The square wave shows schematically how the phase is retarded or advanced at the phase screens.

34

$$c_P + \delta c_P(x,z) = c_{P1}, \tag{89}$$

and in region two let $1 \to 2$ in this expression. Using eq. (30) the argument of the Δ-phase for the P wave is

$$\Delta_m^{(P)}(x) = \begin{cases} \left(\frac{w^2}{c_{P_1}^2} - \left(\frac{m\pi}{2d} \right)^2 \right)^{1/2} \Delta z & \text{if } -d < x < d \\ \\ \left(\frac{w^2}{c_{P_2}^2} - \left(\frac{m\pi}{2d} \right)^2 \right)^{1/2} \Delta z & \text{if } d < x < 3d \end{cases} \tag{90}$$

This is actually a periodic function, which simply repeats for the other regions. We shall express the Δ-phase as the Fourier series

$$e^{i\Delta_m^{(P)}(x)} = \sum_n D_{mn}^{(P)} e^{in\pi z/2d}, \tag{91}$$

where for $n = 0$

$$D_{m0}^{(P)} = \frac{1}{2} \left\{ e^{i\left(\frac{w^2}{c_{P_1}^2} - \left(\frac{m\pi}{2d} \right)^2 \right)^{1/2} \Delta z} + e^{i\left(\frac{w^2}{c_{P_2}^2} - \left(\frac{m\pi}{2d} \right)^2 \right)^{1/2} \Delta z} \right\}, \tag{92}$$

and for $n \neq 0$

$$D_{mn}^{(P)} = \frac{1}{2} \left\{ e^{i\left(\frac{w^2}{c_{P_1}^2} - \left(\frac{m\pi}{2d} \right)^2 \right)^{1/2} \Delta z} - e^{i\left(\frac{w^2}{c_{P_2}^2} - \left(\frac{m\pi}{2d} \right)^2 \right)^{1/2} \Delta z} \right\} \frac{\sin n\pi/2}{n\pi/2}. \tag{93}$$

There are also similar results for the S wave with $P \to S$ in the expressions above.

Inserting the Δ-phases into the expressions derived in eqs. (46-49) produces the recursion matrix for this problem. Recall that the Fourier coefficients in the matrix formulation have been rescaled according to (38) and (39). In terms of the notation used here, the elements of this matrix are

35

$$U_{mn}^{PP} = \sqrt{\frac{a_m}{a_n}} \frac{a_n d_m + b_m c_n}{a_m d_m + b_m c_m} D_{n,m-n}^{(P)} \tag{94}$$

$$U_{m\nu}^{PS} = \sqrt{\frac{c_P a_m}{c_S d_\nu}} \frac{b_m d_\nu - b_\nu d_m}{a_m d_m + b_m c_m} D_{\nu,m-\nu}^{(S)} \tag{95}$$

$$U_{\mu n}^{SP} = \sqrt{\frac{c_S d_\mu}{c_P a_n}} \frac{c_n a_\mu - c_\mu a_n}{a_\mu d_\mu + b_\mu c_\mu} D_{n,\mu-n}^{(P)} \tag{96}$$

$$U_{\mu\nu}^{SS} = \sqrt{\frac{d_\mu}{d_\nu}} \frac{a_\mu d_\nu + b_\nu c_\mu}{a_\mu d_\mu + b_\mu c_\mu} D_{\nu,\mu-\nu}^{(S)}. \tag{97}$$

Note that if the velocities are the same in the two regions, $D_{n,m-n}^{(P)}$ and $D_{n,m-n}^{(S)}$ both vanish for $n \neq m$, and there is no conversion of wave type.

To completely specify the solution, the initial coefficients must be given that correspond to the initial disturbance at $z = 0$. To correspond to the (even,odd) parity initial condition of the exact solution given in eq. (73), the initial coefficients are

$$A_m^{(0)} = 0 \tag{98}$$

$$B_m^{(0)} = \delta_{m,0}, \tag{99}$$

and for the (odd,even) parity initial condition of eq. (86), let $A_m^{(0)} \leftrightarrow B_m^{(0)}$ in these two expressions.

As discussed for the exact solution, for any other initial conditions independent of x, linear superpositions of these expressions may be used because of the linearity of the wave equation. For initial conditions that do depend on x, elementary Fourier analysis may be used to determine the initial coefficients.

In principle, the phase screen solution for the medium we are interested in is complete. To actually obtain the displacement after N phase screens requires numerical work to iterate the recursion relations N times. We will numerically compare the phase-screen solution to the exact solution in the next section.

36

3.3 COMPARISON OF THE SOLUTIONS

To compare the two solutions requires numerical routines to obtain both solutions, and a method of comparison. Although there are many ways we could compare the two answers, we have chosen to do so in the following two ways. First, the cartesian components of the two displacement vectors at fixed values of z are plotted. Also, the average difference of the vectors at fixed z is computed. Explicitly, this means that the absolute norm of the difference of the vectors is computed at a given value of z, integrated over x, and divided by the length of the interval to obtain the average difference.

Before proceeding with these comparisons, the marginal number of phase screens, discussed in chapter two, must be calculated. For this periodic problem the Cauchy criterion derived in eq. (33) becomes

$$
\begin{aligned}
ANSD(z_f) \ &= \ \frac{1}{4d}\int_{-d}^{3d} dx \|\mathbf{u}^{(M)}(x,z_f) - \mathbf{u}^{(M-K)}(x,z_f)\|^2 \\
&= \ \sum_m \left\{ |u_{xm}^{(M)}(z_f) - u_{xm}^{(M-K)}(z_f)|^2 + |u_{zm}^{(M)}(z_f) - u_{zm}^{(M-K)}(z_f)|^2 \right\} \\
&\le \ tolerance,
\end{aligned}
\tag{100}
$$

where

$$
u_m^{(M)}(z_f) = c_m A_m^{(M)} e^{i\omega a_m z_f / c_P (M+1)} + d_m B_m^{(M)} e^{i\omega d_m z_f / c_S (M+1)}
\tag{101}
$$

$$
u_m^{(M)}(z_f) = a_m A_m^{(M)} e^{i\omega a_m z_f / c_P (M+1)} - b_m B_m^{(M)} e^{i\omega d_m z_f / c_S (M+1)}.
\tag{102}
$$

Note that for M phase screens evenly distributed over a distance z_f, $\Delta z = z_f/(M+1)$. We have chosen the tolerance to be 0.005 for the following results, and incremented the number of phase screens by adding 10 for every 50 km of observation distance, i. e. $K = 0.2z_f$ is used in eq. (100). Tables 1 and 2 contain the MNPS results for a series of observation distances using various combinations of the frequency, width, and magnitude of velocity fluctuations.

From these tables a general guideline for the number of phase screens to be used may be extracted;

37

Table 1. Marginal number of phase screens for $c_{S_1} = 3.6$ km/s, $c_{S_2} = 3.8$ km/s, $c_P/c_S = \sqrt{2}$.

w (rad/s)	z_f (km) d (km)	50	100	200	400
5.0	10.0	50	100	200	400
2.5	10.0	60	160	320	800
10.0	5.0	100	200	400	960
5.0	5.0	160	320	800	1600
10.0	2.5	320	800	1600	3840

Table 2. Marginal number of phase screens for $c_{S_1} = 3.5$ km/s, $c_{S_2} = 3.9$ km/s, $c_P/c_S = \sqrt{2}$.

w (rad/s)	z_f (km) d (km)	50	100	200	400
5.0	10.0	170	340	680	1360
10.0	5.0	340	680	1360	3360
2.5	10.0	240	480	960	2560
5.0	5.0	480	960	2560	5120
10.0	2.5	320	640	1600	3200

$$MNPS = \alpha \frac{L}{kd^2} \left(\frac{\delta c}{\bar{c}} \right)^\beta,$$ (103)

where L is used here to represent the observation distance, $\alpha \sim 2 \times 10^5$ is the constant of proportionality for the tolerance we have chosen, and $\beta \sim 2$. For a less stringent tolerance the number of phase screens needed will be much less.

Using this information, the comparison is made as efficiently as possible. The parameter space to be examined includes the magnitude of the velocity fluctuations and three length scales, the wavelength, the width of the regions, and the observation distance. One of these length scales may be eliminated, however, by noting that the solution is invariant under rescaling all of the lengths by the same factor. Thus we are free to fix the wavelength and vary the remaining parameters.

Figures 5-16 contain plots of the real parts of the cartesian components of the phase-screen and exact displacement vectors, both in the same figures, at a sequence of observation distances. The solid lines correspond to the exact solution while the dashed lines correspond to the phase-screen solution; the x-component of the displacement is plotted above the z-component. Also, the average of the difference of the norm of the two vector solutions has been included in the figure captions. For all of these comparisons $c_P/c_S = \sqrt{2}$, which was chosen to simplify the analysis of the exact solution.

These comparisons demonstrate the accuracy and qualitative features of the method, although we have included only a small sampling. For example, it is clear that the accuracy of the method decreases for larger observation distances and smaller widths, as compared with the wavelength, and for larger velocity perturbations. Further analysis shows that the quantitative conditions for the method to be valid are

$$kd > 1,$$ (104)

such that backscattering is small, and

$$\frac{L}{kd^2} \left(\frac{\delta c}{\bar{c}} \right)^\beta < 1,$$ (105)

where again $\beta \sim 2$ for the parameters we are using. This latter condition is very similar to a geometrical optics condition, and is demonstrated by comparing figures 5-
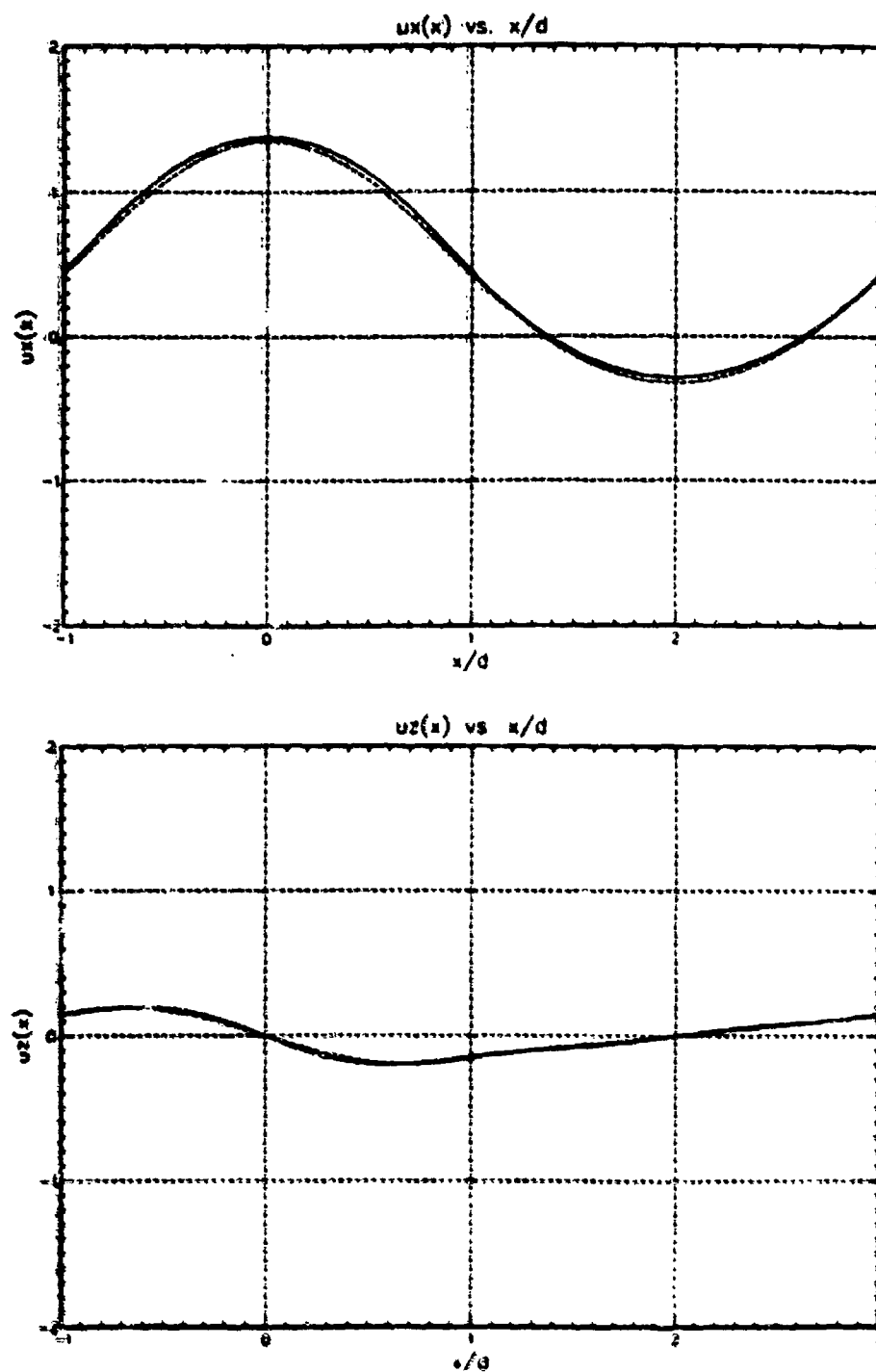
39

Figure 5. Comparison of the exact and phase-screen solutions for $w = 5.0$ rad/s, $\bar{c}_S = 3.7$ km/s, $d = 5.0$ km, $\delta c_S = 0.1$ km/s, $z_f = 50.0$ km, ave. diff. $= 0.029$.

40
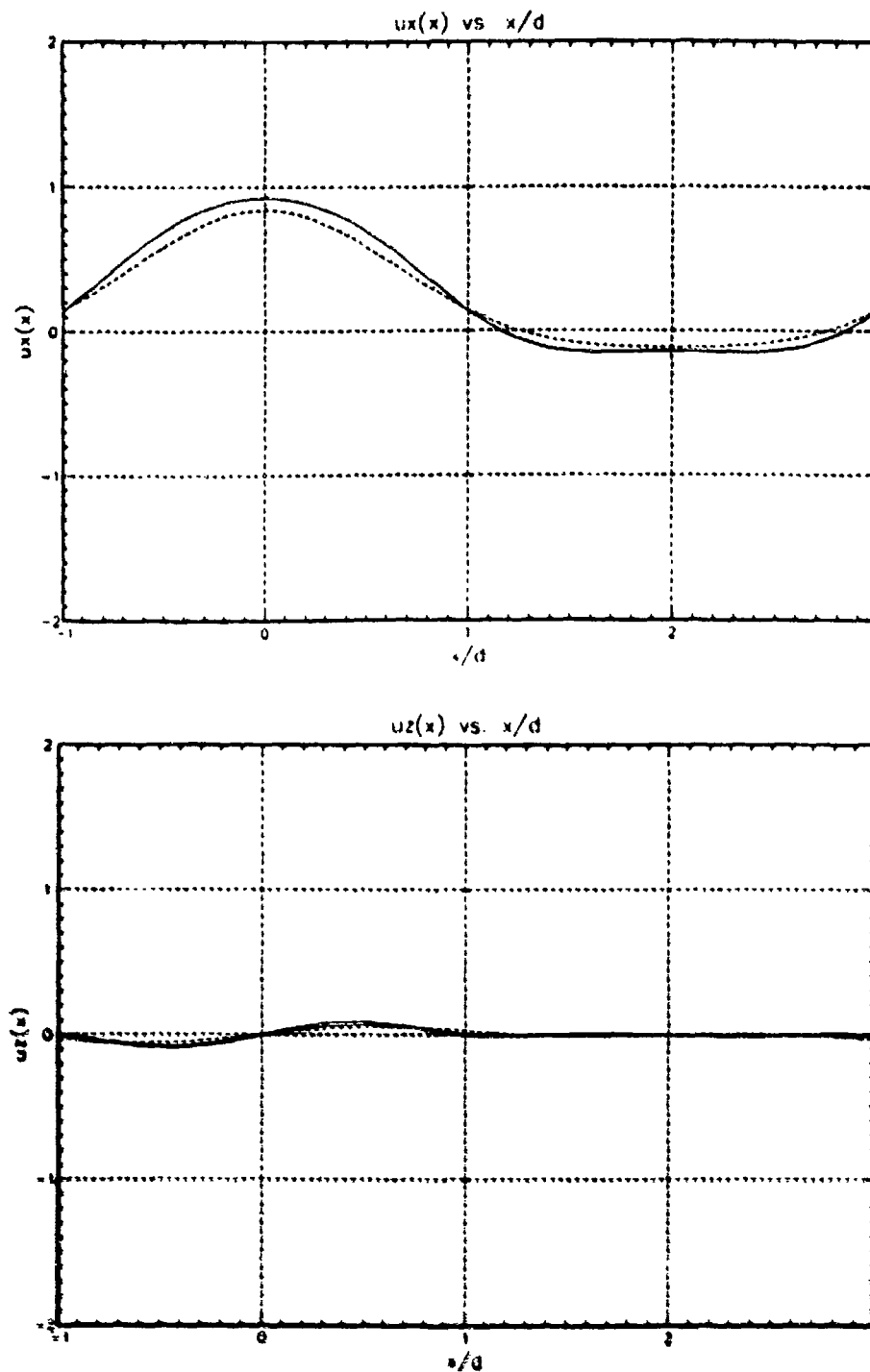
Figure 6. Comparison of the exact and phase-screen solutions for $w = 5.0$ rad/s, $\bar{c}_S = 3.7$ km/s, $d = 5.0$ km, $\delta c_S = 0.1$ km/s, $z_f = 100.0$ km, ave. diff. $= 0.048$.

41
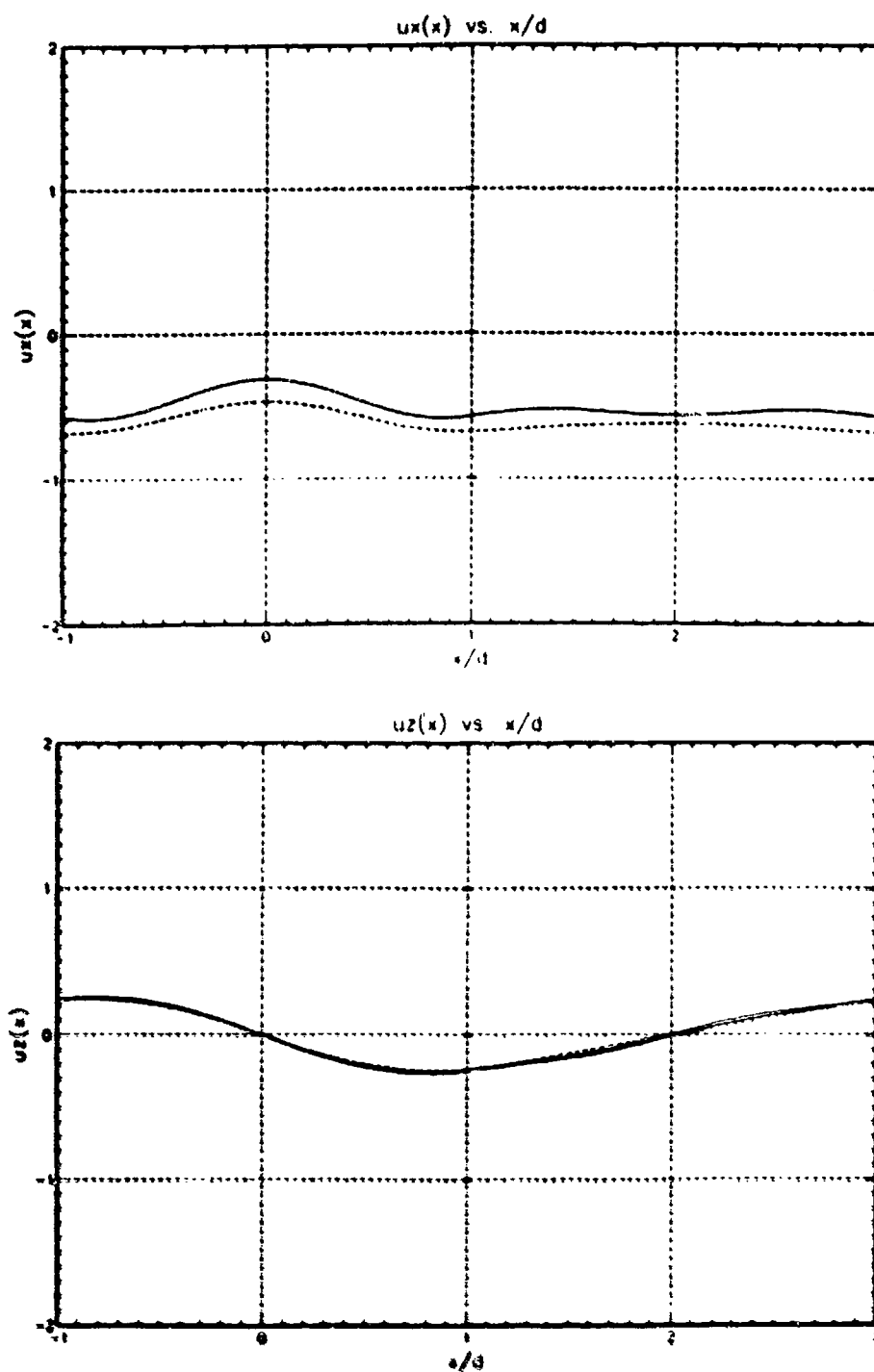
Figure 7. Comparison of the exact and phase-screen solutions for $w = 5.0$ rad/s, $\bar{c}_S = 3.7$ km/s, $d = 5.0$ km, $\delta c_S = 0.1$ km/s, $z_f = 200.0$ km, ave. diff. $= 0.082$.
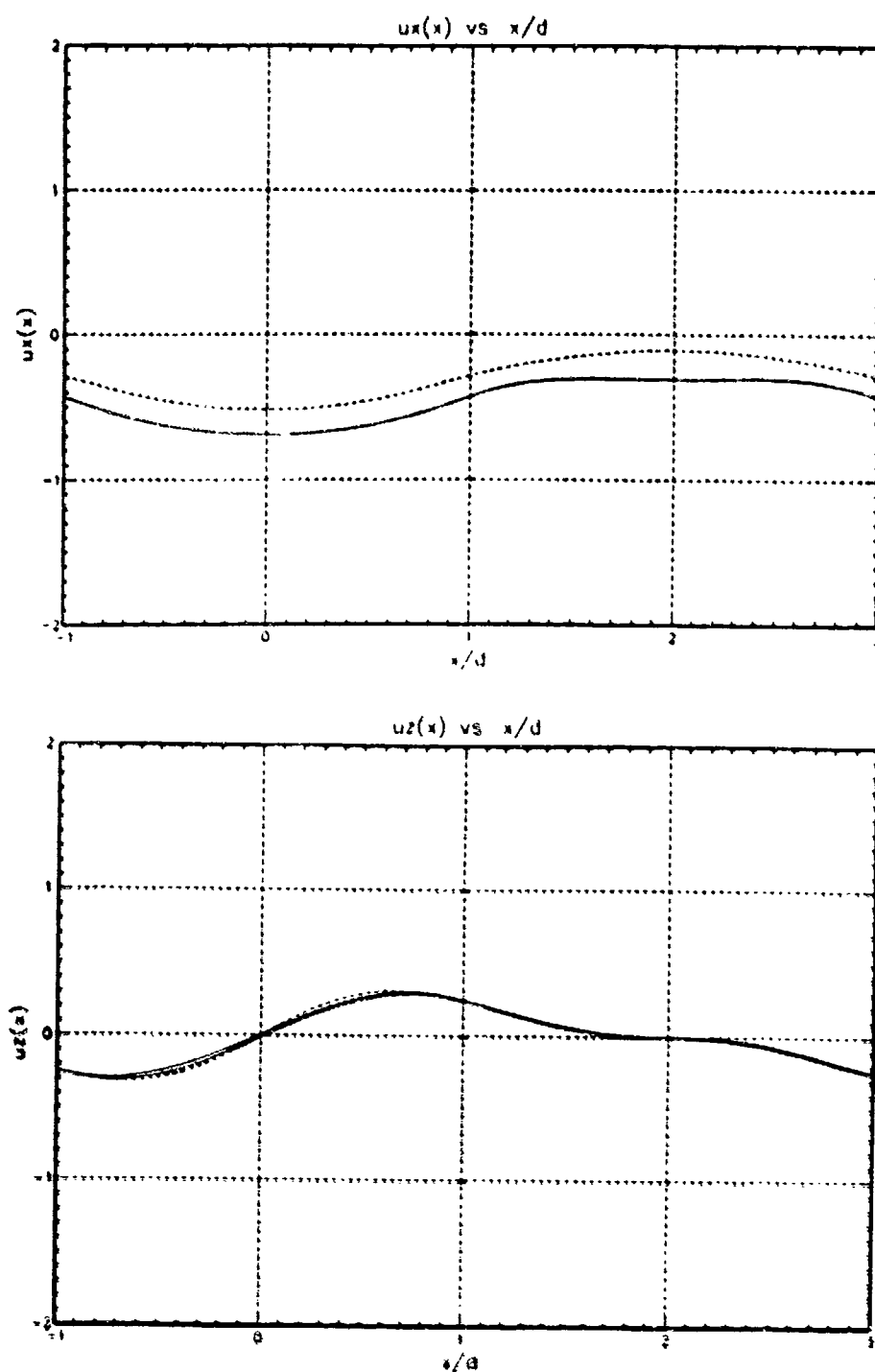
Figure 8. Comparison of the exact and phase-screen solutions for $w = 5.0$ rad/s, $\bar{c}_S = 3.7$ km/s, $d = 5.0$ km, $\delta c_S = 0.1$ km/s, $z_f = 400.0$ km, ave. diff. $= 0.141$.

43
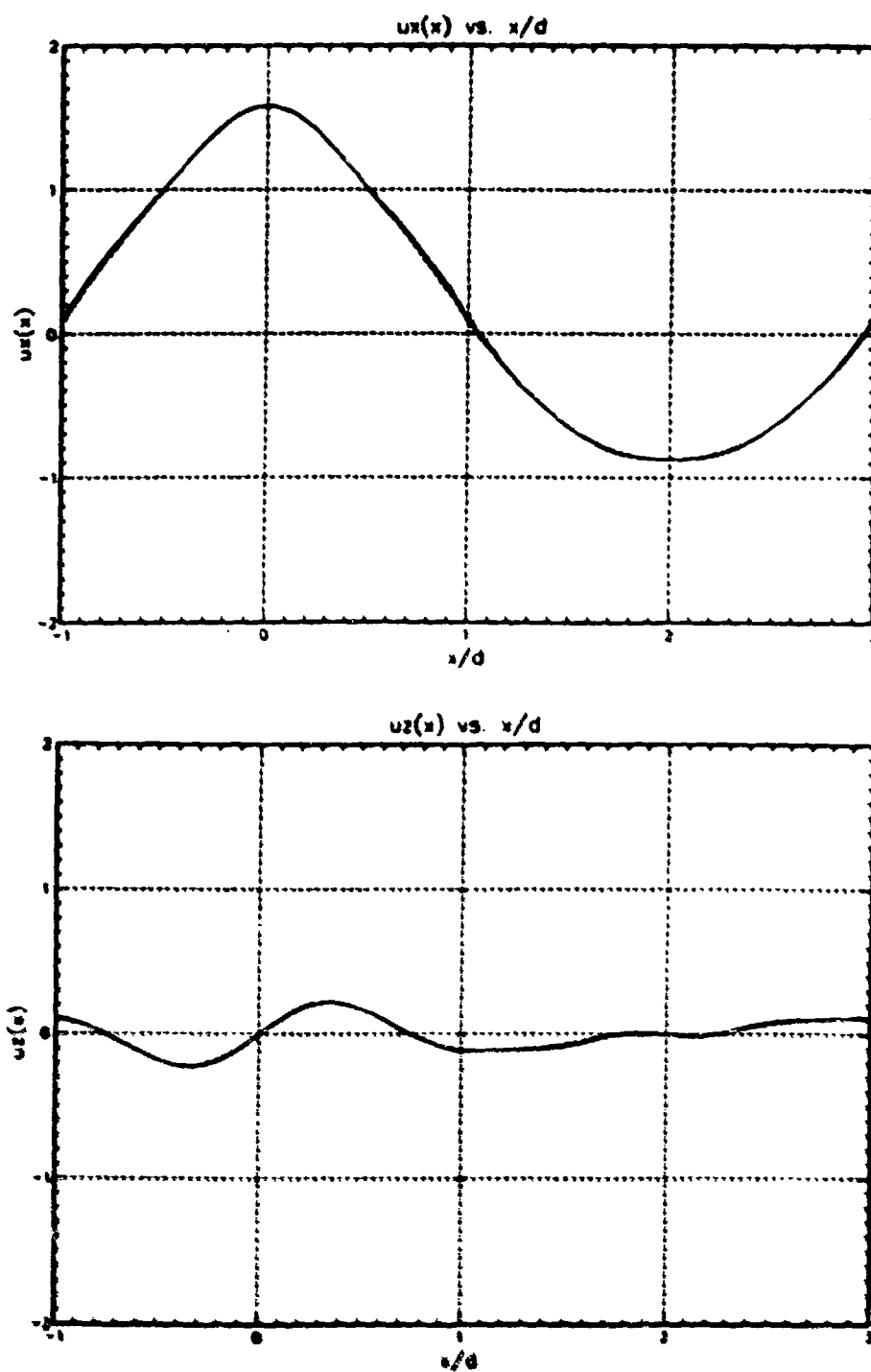
Figure 9. Comparison of the exact and phase-screen solutions for $w = 5.0$ rad/s, $\bar{c}_s = 3.7$ km/s, $d = 10.0$ km, $\delta c_s = 0.1$ km/s, $z_f = 50.0$ km, ave. diff. $= 0.019$.

44
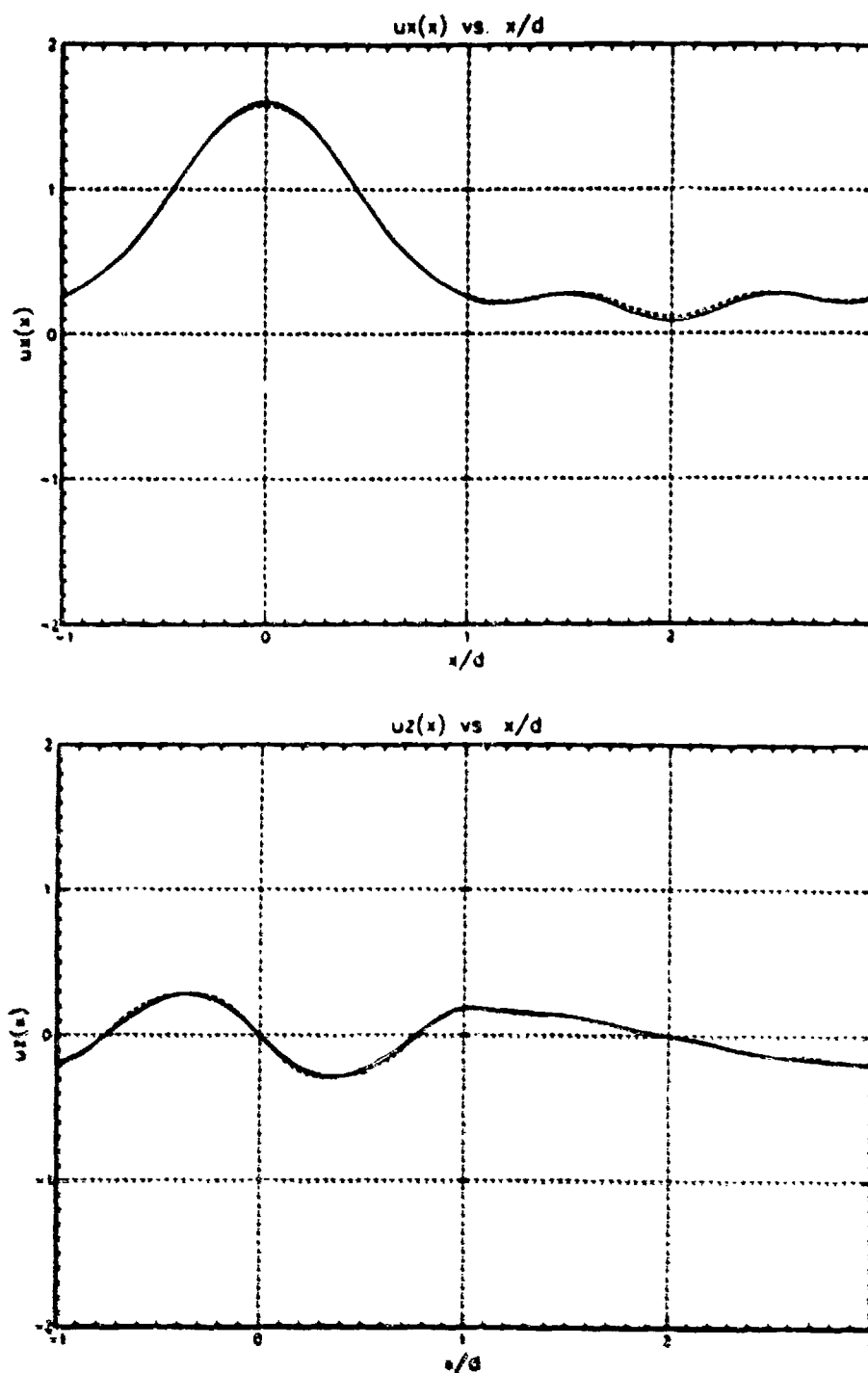
Figure 10. Comparison of the exact and phase-screen solutions for $w = 5.0$ rad/s, $\bar{c}_s = 3.7$ km/s, $d = 10.0$ km, $\delta c_s = 0.1$ km/s, $z_f = 100.0$ km, ave. diff. $= 0.024$.
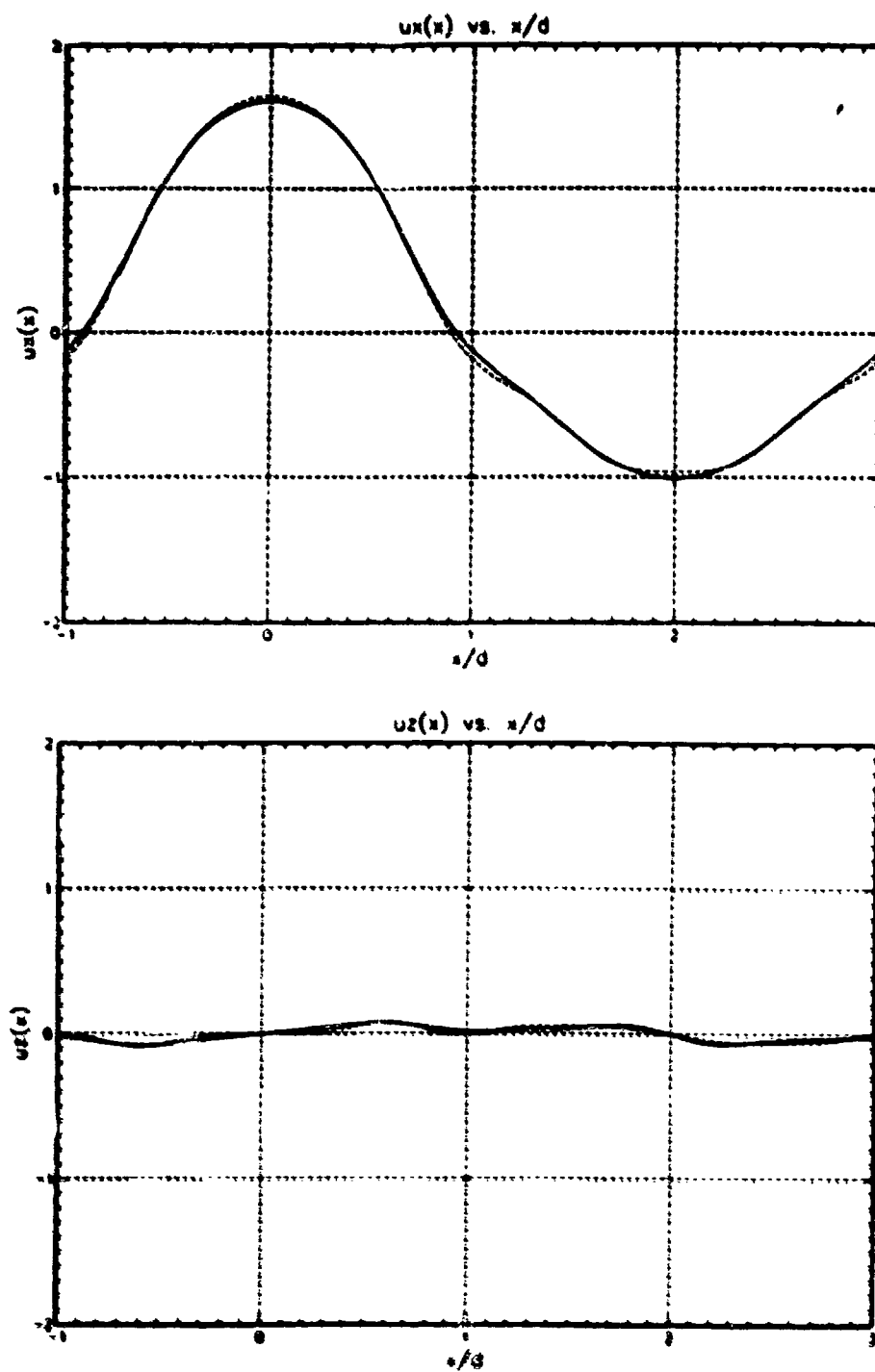
45

Figure 11. Comparison of the exact and phase-screen solutions for
$w = 5.0$ rad/s, $\bar{c}_s = 3.7$ km/s, $d = 10.0$ km, $\delta c_s = 0.1$ km/s,
$z_f = 200.0$ km, ave. diff. $= 0.029$.

Figure 12. Comparison of the exact and phase-screen solutions for $w = 5.0$ rad/s, $\bar{c}_S = 3.7$ km/s, $d = 10.0$ km, $\delta c_S = 0.1$ km/s, $z_f = 400.0$ km, ave. diff. = 0.046.

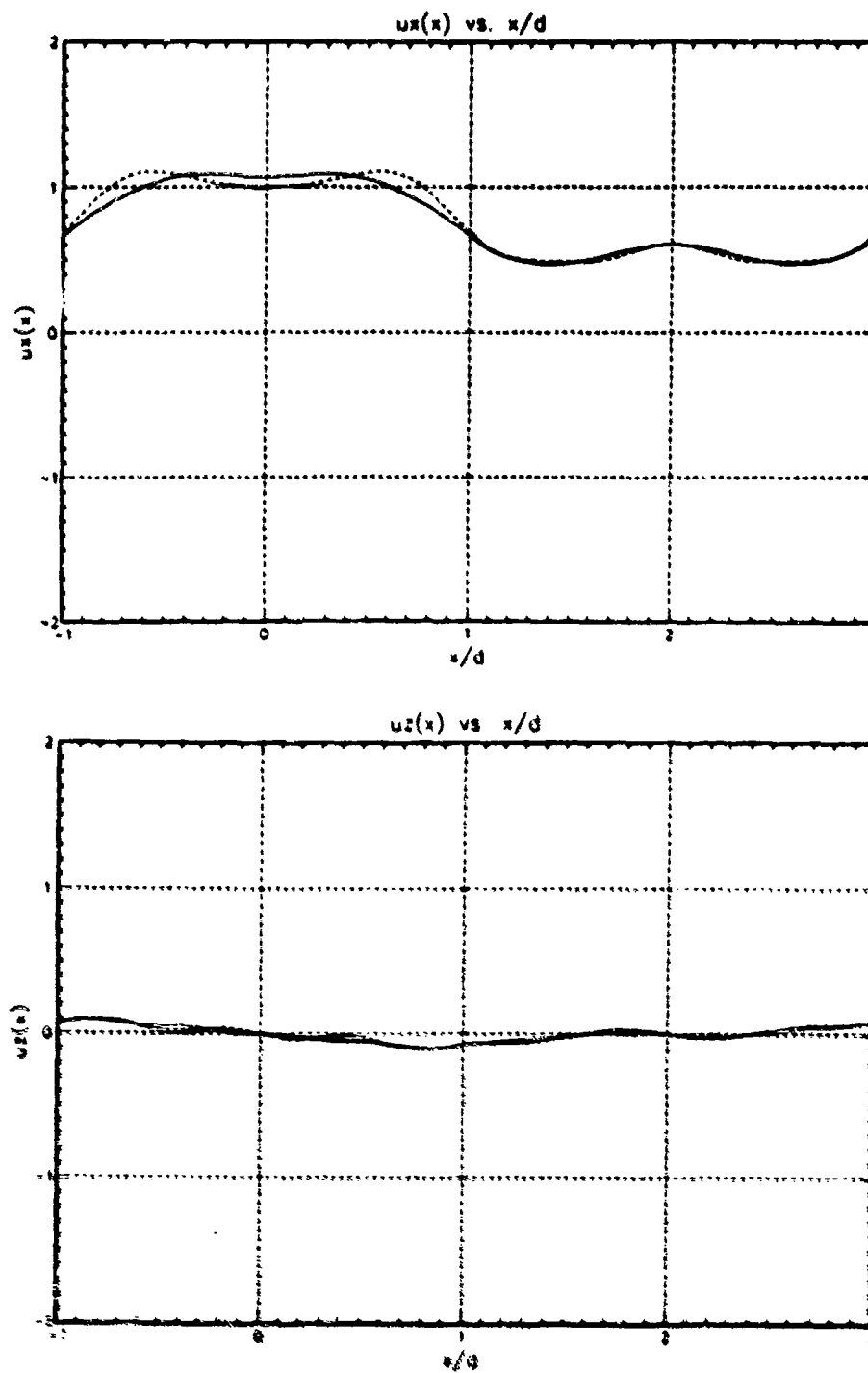**Figure 13.** Comparison of the exact and phase-screen solutions for $w = 5.0$ rad/s, $\bar{c}_S = 3.7$ km/s, $d = 10.0$ km, $\delta c_S = 0.2$ km/s, $z_f = 50.0$ km, ave. diff. $= 0.035$.

48
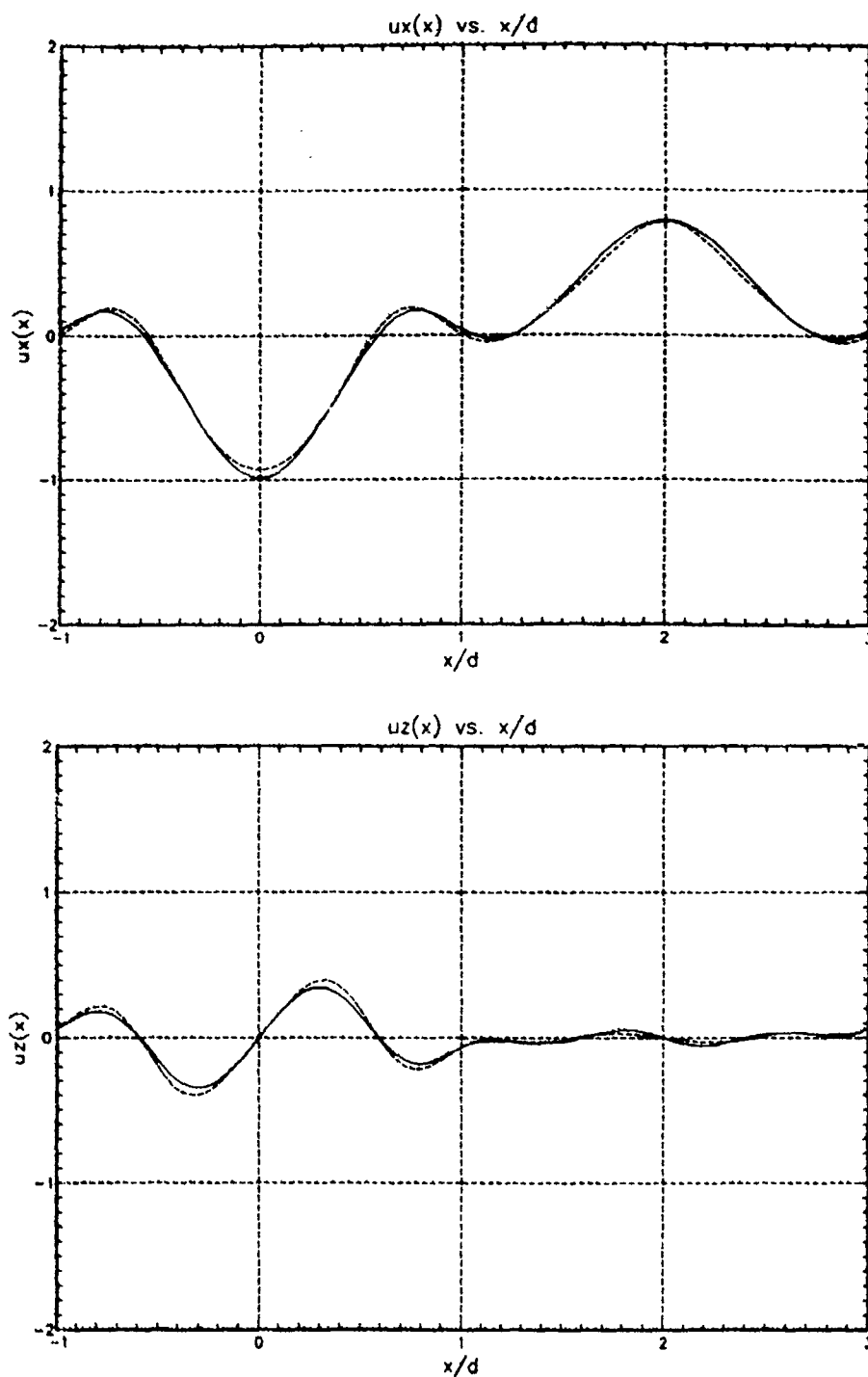
Figure 14. Comparison of the exact and phase-screen solutions for $w = 5.0$ rad/s, $\bar{c}_S = 3.7$ km/s, $d = 10.0$ km, $\delta c_S = 0.2$ km/s, $z_f = 100.0$ km, ave. diff. $= 0.050$.

49

Figure 15. Comparison of the exact and phase-screen solutions for $w = 5.0$ rad/s, $\bar{c}_\beta = 3.7$ km/s, $d = 10.0$ km, $\delta c_\beta = 0.2$ km/s, $z_f = 200.0$ km, ave. diff. $= 0.066$.
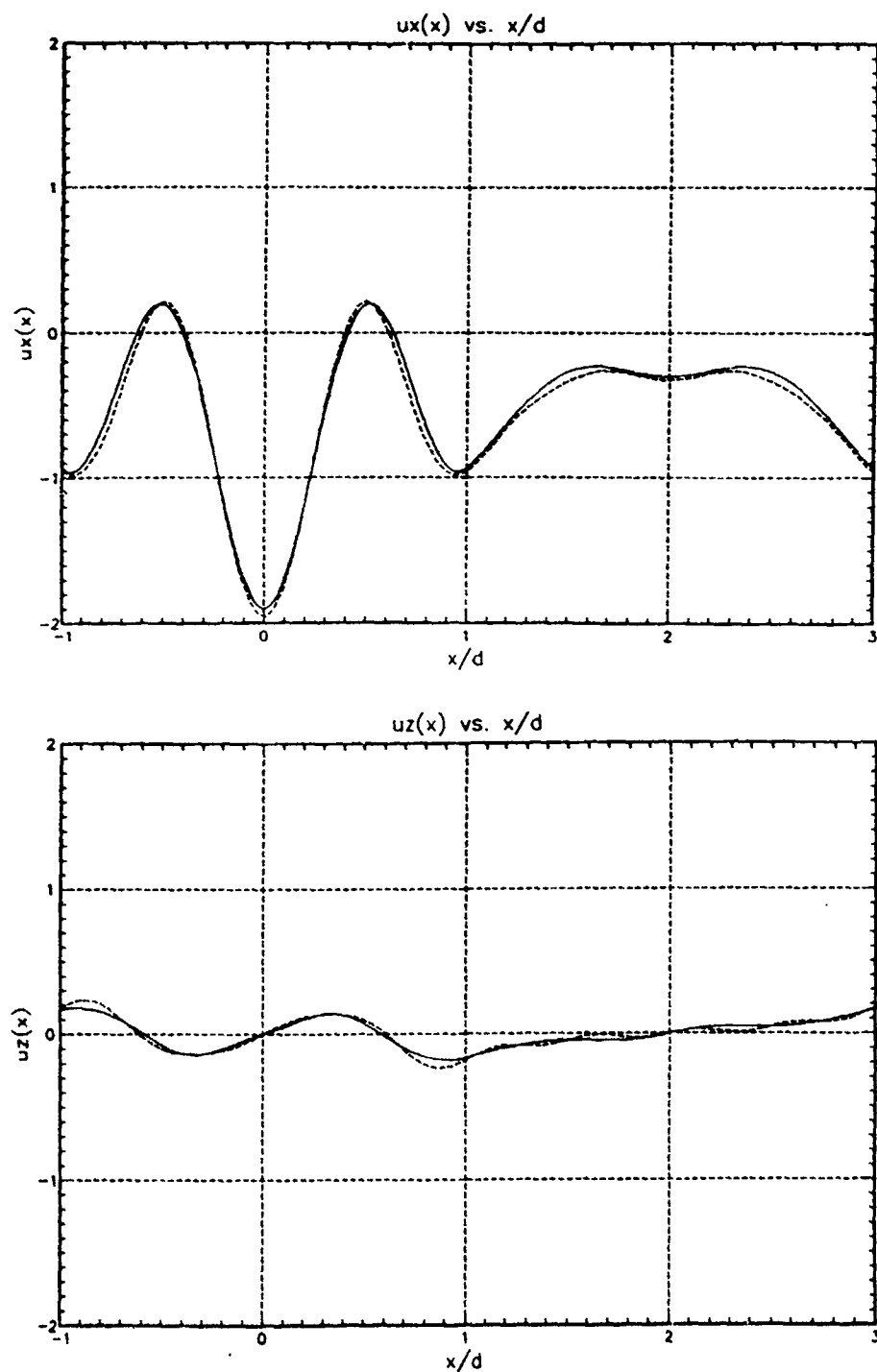
Figure 16. Comparison of the exact and phase-screen solutions for
$w = 5.0$ rad/s, $\bar{c}_S = 3.7$ km/s, $d = 10.0$ km, $\delta c_S = 0.2$ km/s,
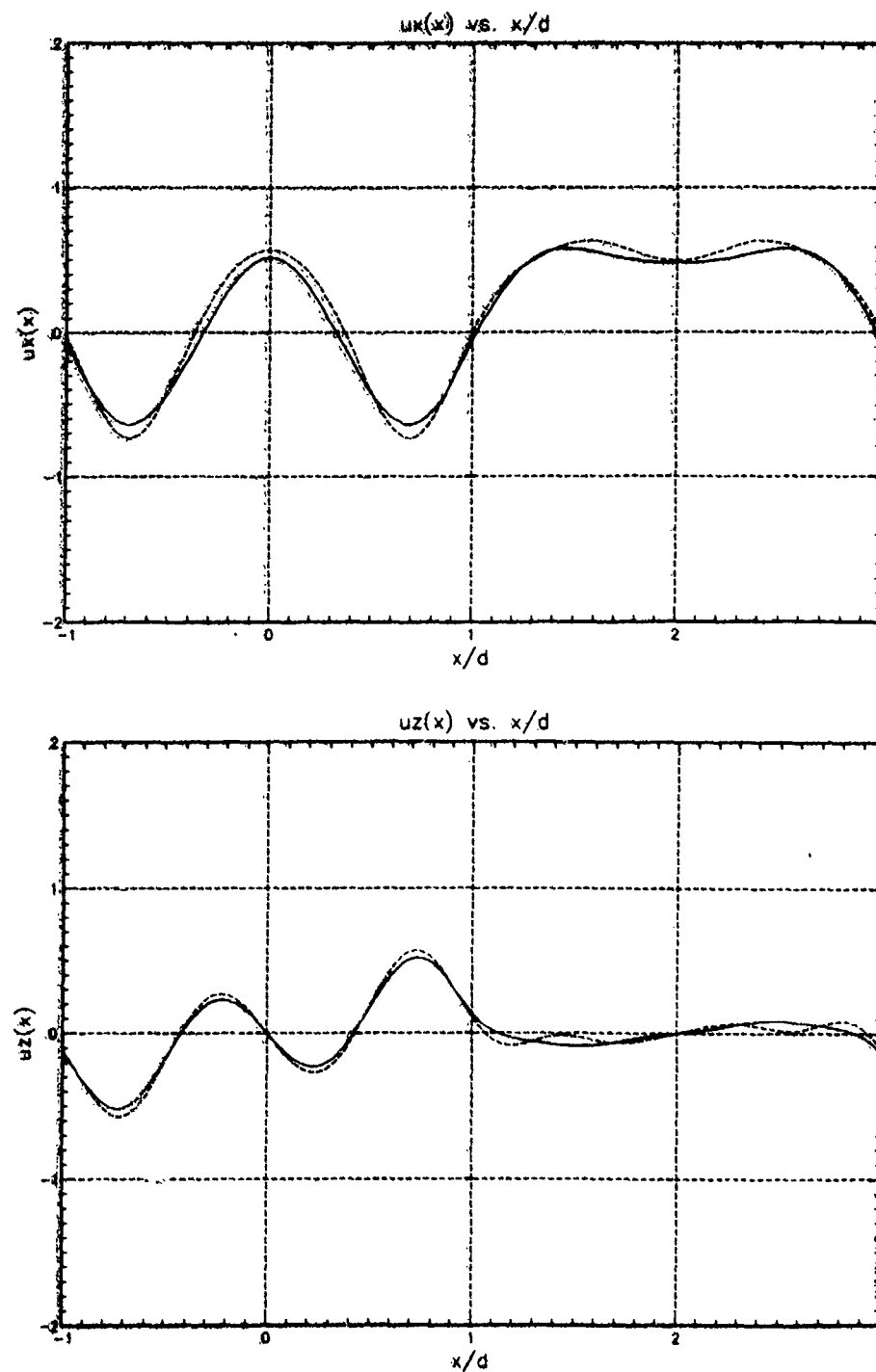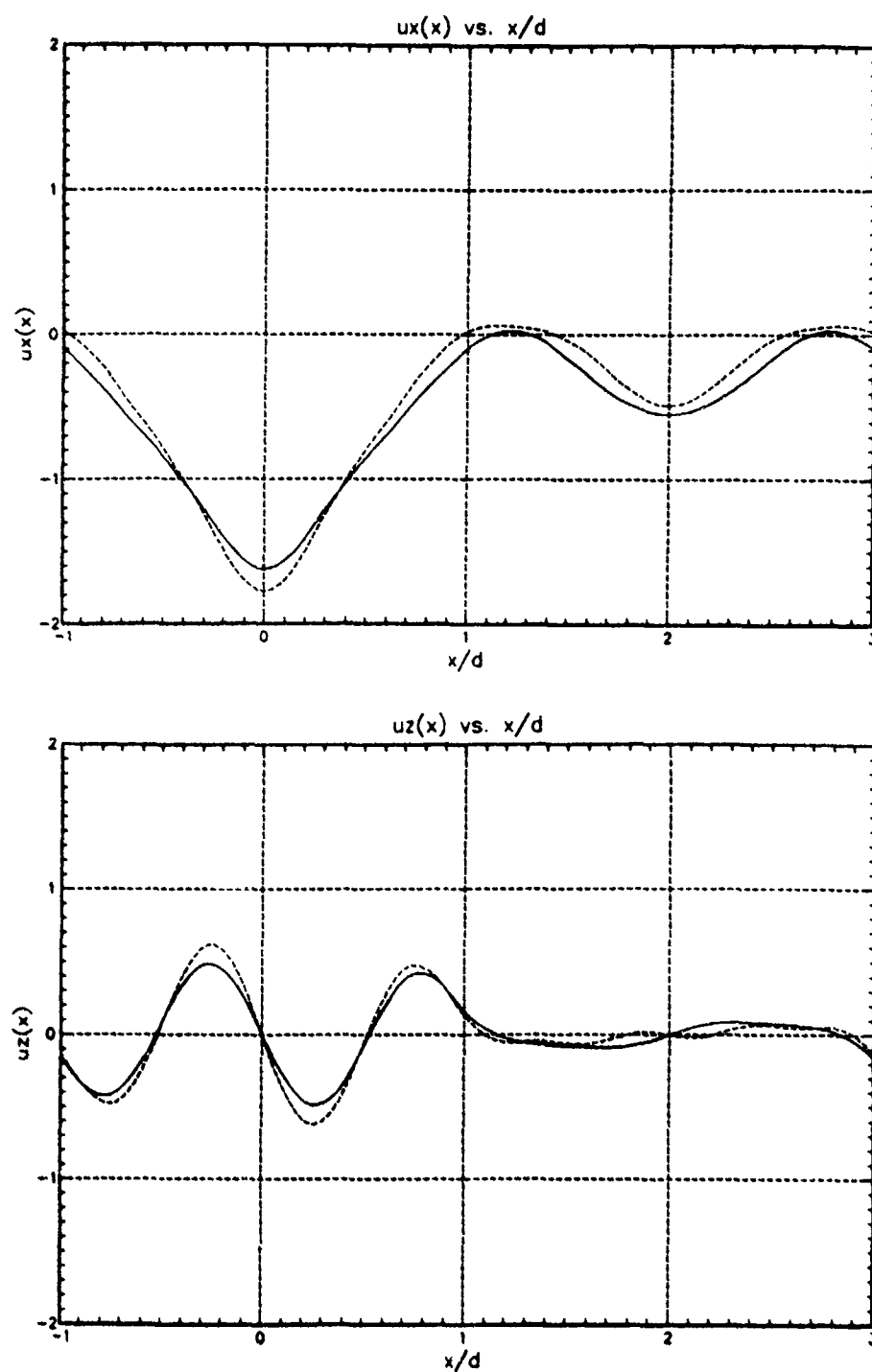$z_f = 400.0$ km, ave. diff. $= 0.114$.

51

condition, and is demonstrated by comparing figures 5-8 to 9-12. Since the width in the latter figures was doubled, the displacement may be propagated to four times the distance at the same accuracy. Also, comparing figures 9-12 to 13-16 demonstrates that that doubling the velocity fluctuation reduces the observation distance by a factor of four to maintain the same accuracy. These relations have been verified by other similar comparisons.

3.4 ENERGY CONVERSION

We conclude this chapter with an examination of the parameters that induce the maximum conversion of energy from one type of wave to another. To accomplish this we maximize the energy conversion across a single phase screen for an incident plane wave. The dependence of conversion on the velocity fluctuations comes from the Fourier coefficients of the Δ-phases, given in eqs. (92,93); the absolute value squared of these coefficients enter into the expression for the energy. These factors are bounded from above regardless of the magnitude of the velocity perturbations, and satisfy

$$|D_{m0}|^2 < 1 \tag{106}$$

$$|D_{mn}|^2 < \frac{2}{n\pi}. \tag{107}$$

The dependence on the velocity perturbations is eliminated by using the combination of the perturbations and Δz that give the maximum conversion. Using the recursion matrix, given by eqs. (94-97), with the optimum phase amplitude on the screen, the conversion is maximized for various ratios of c_P/c_S with respect to the dimensionless variable

$$\chi = \frac{2dw}{\pi c_P}, \tag{108}$$

where the factor of 2 and π are due to the convention of making each region a distance $2d$ wide.

Table 3 contains the values of χ, labelled χ_{max}, such that the conversion is maximized for various ratios of the sound speeds. It illustrates that the P wave converts energy at a faster rate than the S wave except when the sound speeds are

equal, and that the length scales that induce the most conversion of either type are approximately equal to the wavelength of the P wave. This regime is considered "resonance scattering", and contributes the most to scattering effects; for $\chi \ll 1$ the medium is quasi-homogeneous, while for $\chi \gg 1$ the medium becomes transparent, Wu (1988). The entries of $\chi_{max} = 1.00$ in table 3(a) are due to the fact that the conversion is maximized as this dimensionless variable gets smaller, but for $\chi < 1.0$, $M_P = 0$ (cf. section 2.4), and the recursion matrix becomes trivial, not admitting conversion. Finally, note that as the ratio c_P/c_S increases, the P wave loses energy more rapidly, while the S wave loses energy more slowly.

Table 3. Maximum energy conversion from one phase screen for an initial (a) P-wave, (b) S-wave.

(a)

c_P/c_S	1.0	$\sqrt{2}$	2.0	4.0
χ_{max}	1.17	1.00	1.00	1.00
$\bar{S}_{S,z}^{(1)}/\bar{S}_{P,z}^{(0)}$	0.31	0.44	0.58	0.64

(b)

c_P/c_S	1.0	$\sqrt{2}$	2.0	4.0
χ_{max}	1.17	1.11	1.06	1.01
$\bar{S}_{P,z}^{(1)}/\bar{S}_{S,z}^{(0)}$	0.31	0.24	0.21	0.19

53

SECTION 4

RANDOM MEDIA

Here we apply the phase-screen method to media for which the position dependent velocity anomalies, $\delta c_P(x, y, z)$ and $\delta c_S(x, y, z)$, are characterized statistically. They will be treated as zero mean random variables. Eventually we will employ phase screens with multiple wavelengths to describe random inhomogeneities on a variety of length scales. The random phases for this problem may be computed in terms of the power spectral density (PSD) of the medium, Knepp [1983] and Martin and Flatté [1988], but this will not be done here. Instead we will limit ourselves to one length scale to obtain the results that follow.

To model a random medium with only one characteristic length scale we use the same periodic phase screens as were used in the previous chapter, aligned over some correlation length, but then randomly shifted by some distance less than the wavelength of the screen in the x-direction, over the next correlation length. This process is then repeated to propagate the wave to the observation point of interest. The number of phase screens used per propagation distance for the random medium problem will be the same as the MNPS determined for the layered problem, for particular values of the widths of the regions, frequencies, mean velocities, etc.

In general, a random shift in the alignment of the phase screen relative to the positioning of the original one is accomplished by letting

$$\Delta_m(x) \longrightarrow \Delta_m(x - 4d\gamma), \tag{109}$$

where γ is a random number such that $0 < \gamma < 1$. Refering back to eqs. (91-97), the affect of this shift on the recursion matrix is straightforward to determine; the elements of the recursion matrix transform according to

$$U_{mn}^{PP} \longrightarrow U_{mn}^{PP} \, e^{-2\pi i(m-n)\gamma} \tag{110}$$

$$U_{m\nu}^{PS} \longrightarrow U_{m\nu}^{PS} \, e^{-2\pi i(m-\nu)\gamma} \tag{111}$$

54

$$U_{\mu n}^{SP} \longrightarrow U_{\mu n}^{SP} \, e^{-3\pi i(\mu-n)\gamma} \qquad (112)$$

$$U_{\mu \nu}^{SS} \longrightarrow U_{\mu \nu}^{SS} \, e^{-3\pi i(\mu-\nu)\gamma} \qquad (113)$$

where again $-M_P < m, n < M_P$ and $-M_S < \mu, \nu < M_S$.

The transformation that implements the random shift may be represented as a matrix as well, written in block form as

$$\Gamma = \begin{pmatrix} e^{2\pi i m \gamma} \delta_{mn} & 0 \\ & \\ 0 & e^{2\pi i \mu \gamma} \delta_{\mu\nu} \end{pmatrix}. \qquad (114)$$

Note that only the diagonal entries are nonvanishing, and there is no implicit summation in this expression. The transformation law for the recursion matrix under a random shift is then given by

$$U \longrightarrow \Gamma U \Gamma^{-1} \qquad (115)$$

It is easily verified that Γ is a unitary matrix, or orthogonal when expressed in its equivalent real form. Thus we need only modify the recursion matrix U once to make it unitary; all random transformations of the modified recursion matrix will automatically lead to total energy conservation.

For the simulations we perform, the recursion matrix of the problem in chapter 3, given by eqs. (92-97), will be employed. The energy flux, averaged over x and t, is computed as a function of observation distance for a number of realizations. Each realization is specified by a set of computer generated psuedo-random numbers which determine the alignment of the set of phase screens. We shall then ensemble average over realizations to smooth out spurious results. In practice, we shall average over one hundred such realizations.

Figures 17-21 plot the averaged energy flux as a function of distance out to 2000 km, and for a variety of parameters. Although we are not attempting to model the lithosphere here, the length scales and velocity perturbations are roughly those

55

found in the lithosphere at NORSAR, Wu and Aki [1985], where the correlation length is 10 − 20 km and the rms velocity perturbations are 2%-4%. The total energy flux has been normalized to one by dividing by the incident flux. The pairs of figures on each page are produced for identical media, including the particular realizations that are used; the upper figures are for initial P waves, while the lower figures are for initial S waves.

The significant features of energy conversion in this 2D random medium are that the conversion rate

1. for P to S occurs at a faster rate than for S to P;

2. is approximately independent of the frequency for high frequencies;

3. is inversely proportional to the length scale of the medium; and

4. is proportional to the square of the velocity fluctuations.

These results may be qualitatively compared to the Born approximation results obtained by Wu and Aki [1985]. The first result is simply due to the fact that the impedance of the P wave is greater than that of the S wave, and the last three are typical of high frequency scattering. In particular, the lack of frequency dependence is easily seen by noting that the displacement scales inversely with the frequency, but the energy flux is given by the frequency squared times the displacement squared, which does not scale with the frequency.

Finally, the energy plots, particularly figures 20 and 21, illustrate that the energies of the waves tend toward fixed values if propagated far enough. These values are independent of the initial conditions, and the asymptotic ratio of the S wave to P wave energy is roughly c_P/c_S.

For propagation in a 3D random medium, realized in the way described above, the expected result is that the energy will be equally partitioned among the S wave polarizations and weighted according to the ratio of the phase velocities relative to the P wave.
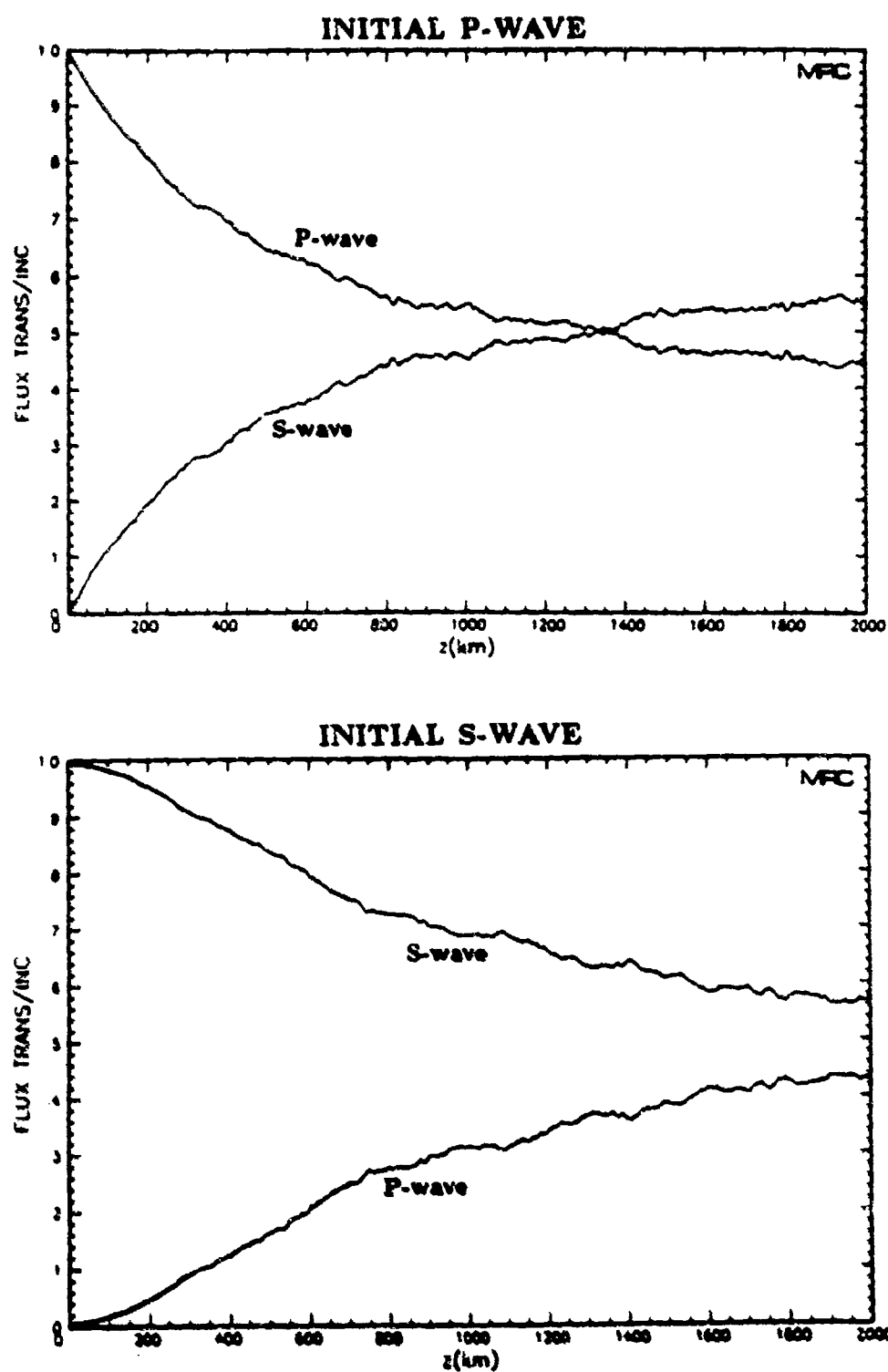
INITIAL P-WAVE

INITIAL S-WAVE

Figure 17.   Energy conversion for a random medium with $w = 5.0$ rad/s, $d = 5.0$ km, $\bar{c}_S = 3.7$ km/s, $\delta c_S = 0.1$ km/s, $c_P/c_S = \sqrt{2}$.

57

INITIAL P-WAVE

INITIAL S-WAVE

Figure 18.   Energy conversion for a random medium with $w = 10.0$ rad/s, $d = 5.0$ km, $\bar{c}_s = 3.7$ km/s, $\delta c_s = 0.1$ km/s, $c_p/c_s = \sqrt{2}$.
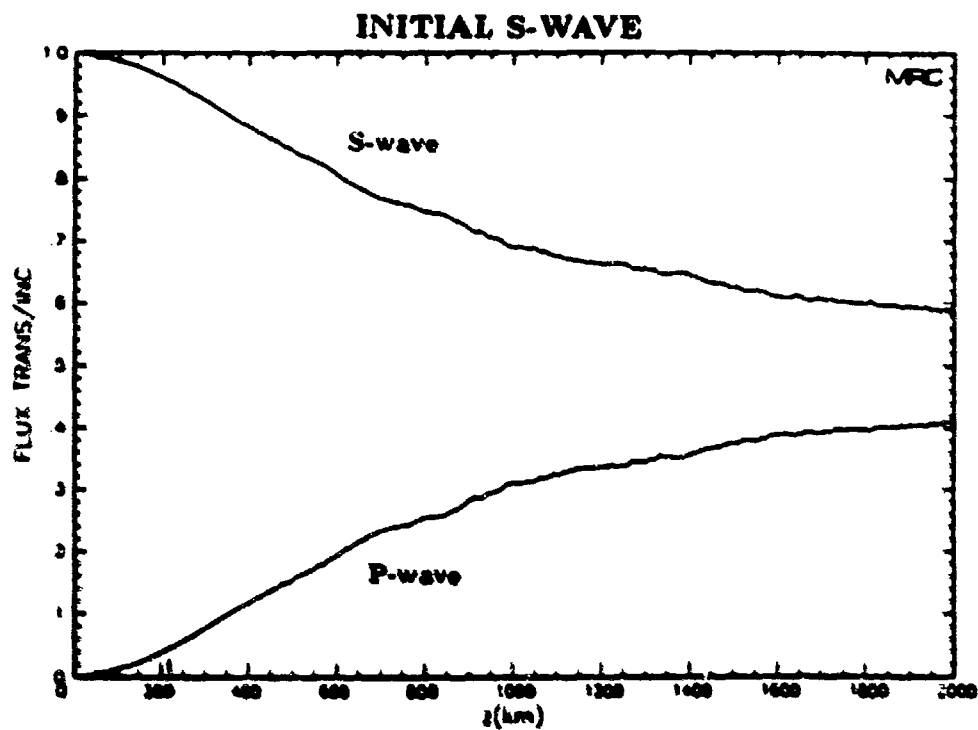
INITIAL P-WAVE

INITIAL S-WAVE

Figure 19. Energy conversion for a random medium with $w = 5.0$ rad/s, $d = 10.0$ km, $\bar{c}_S = 3.7$ km/s, $\delta c_S = 0.1$ km/s, $c_P/c_S = \sqrt{2}$.
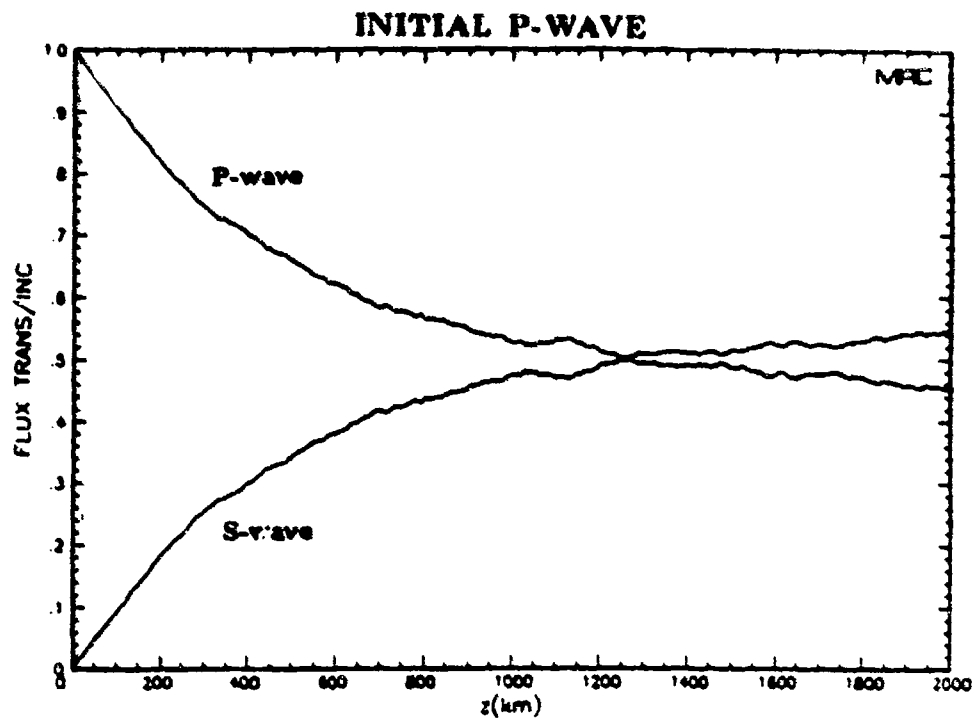
59

INITIAL P-WAVE

INITIAL S-WAVE

Figure 30. Energy conversion for a random medium with $w = 5.0$ rad/s, $d = 5.0$ km, $\bar{c}_S = 3.7$ km/s, $\delta c_S = 0.2$ km/s, $c_P/c_S = \sqrt{2}$.
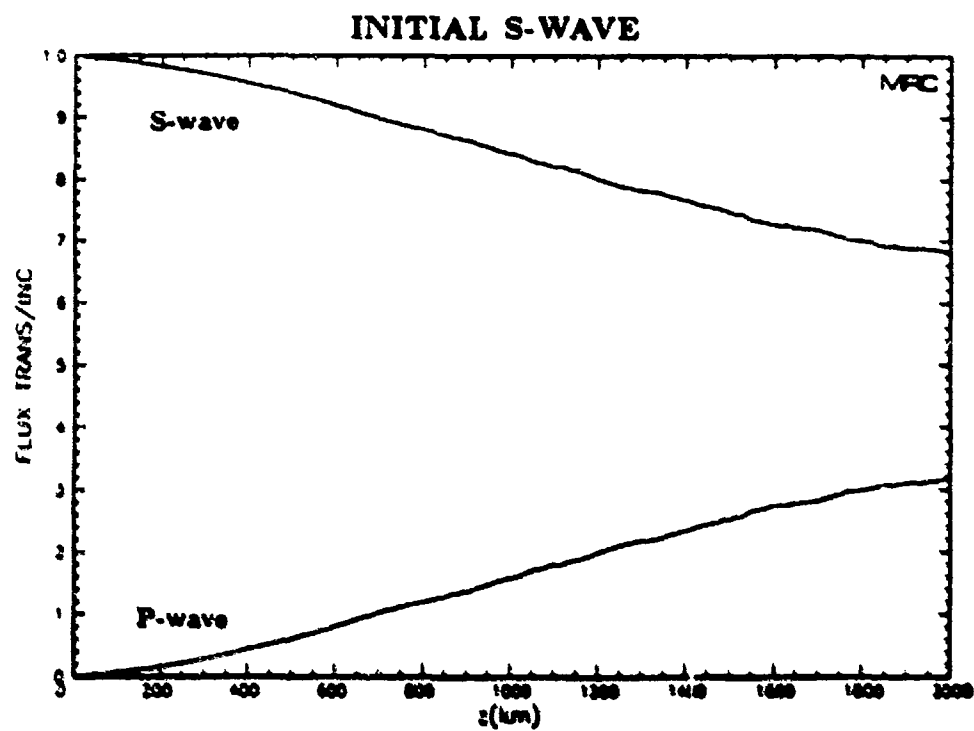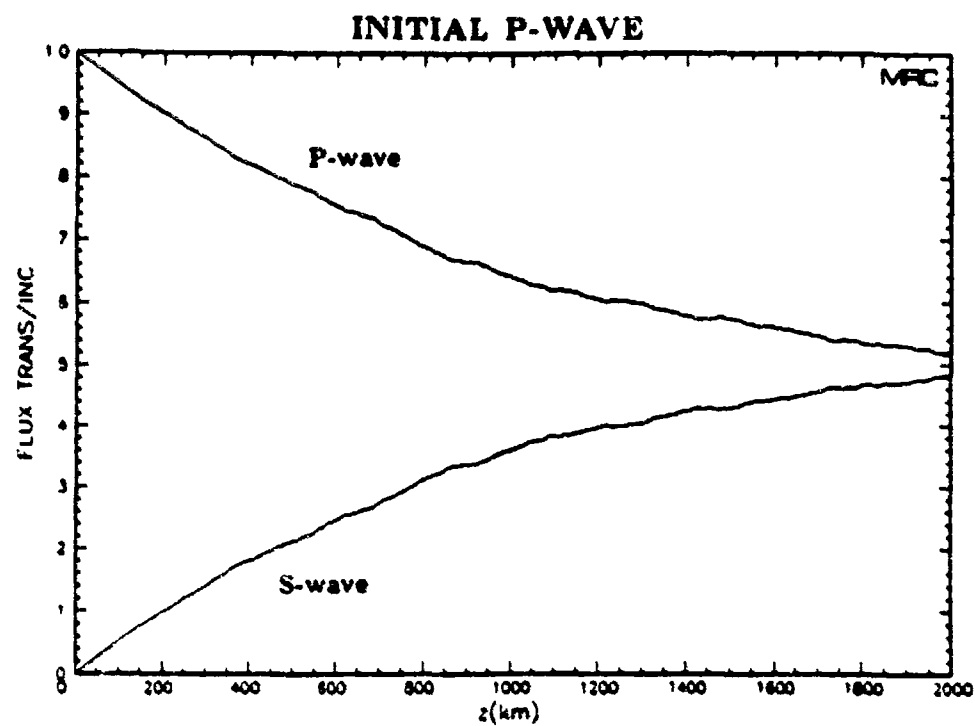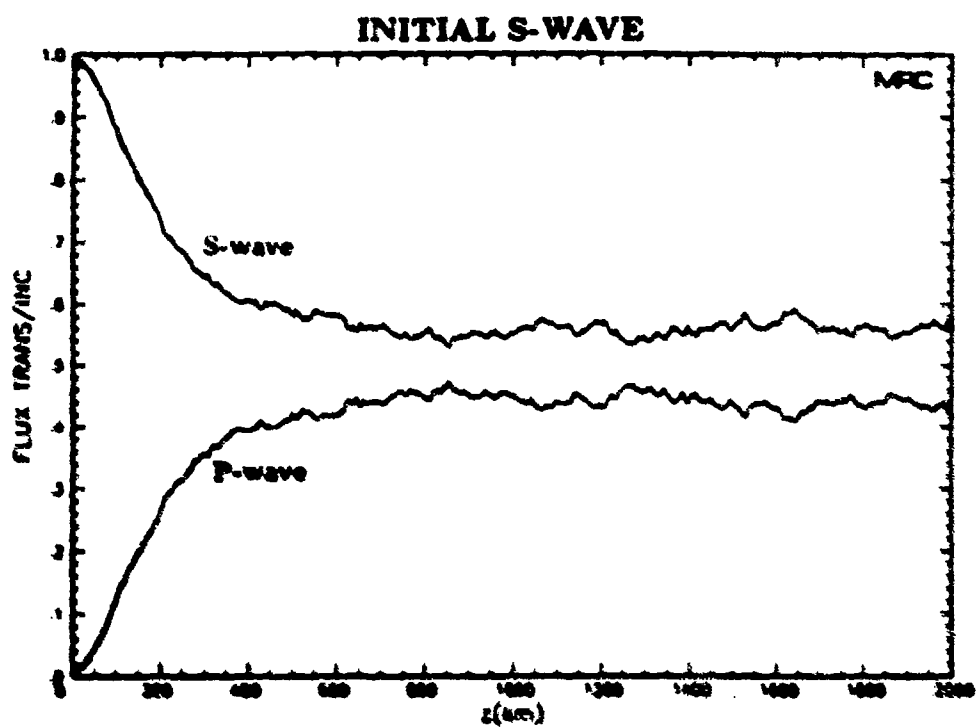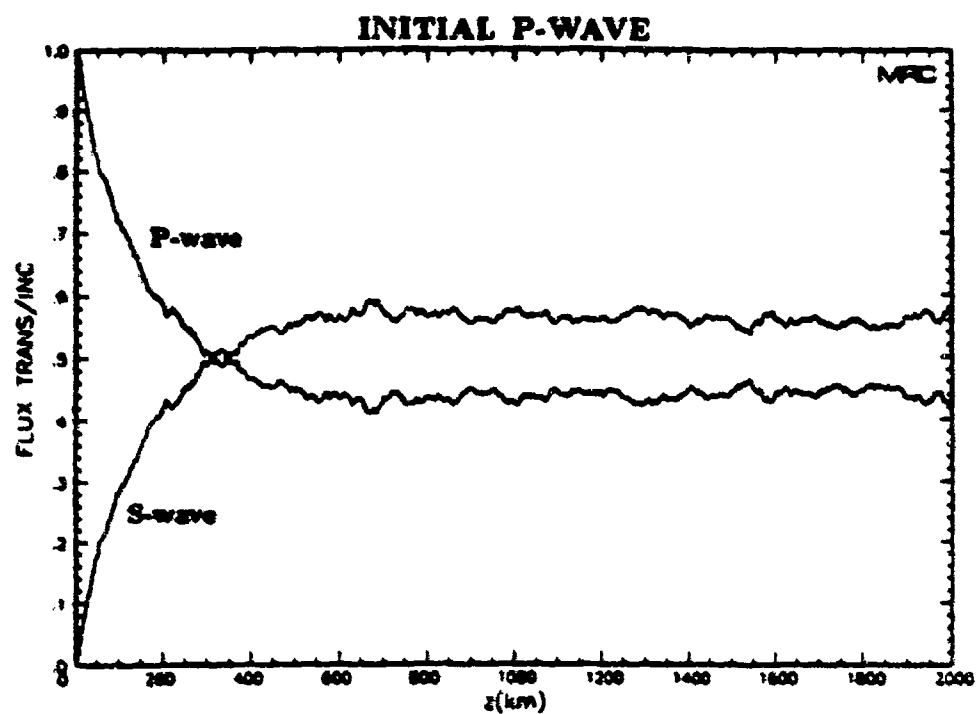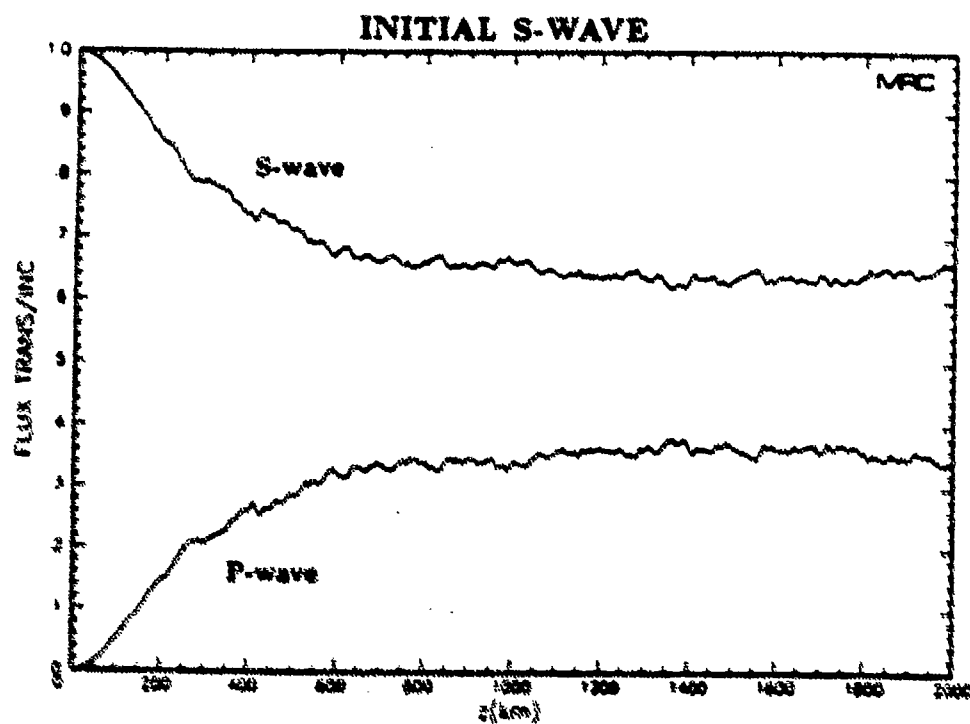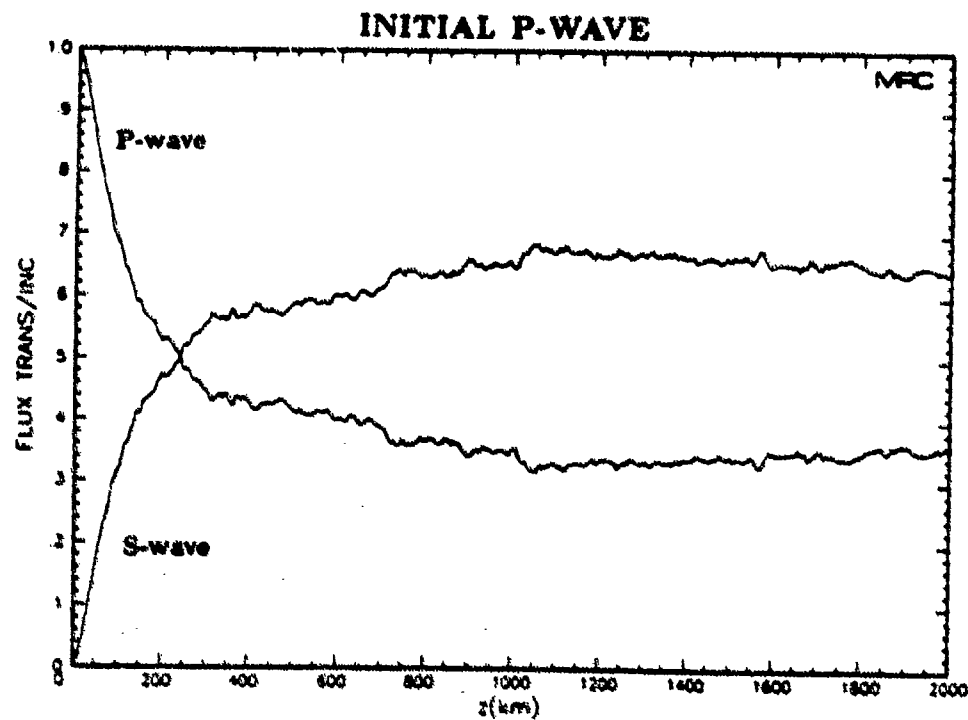
60

INITIAL P-WAVE

INITIAL S-WAVE

Figure 31. Energy conversion for a random medium with $w = 5.0$ rad/s, $d = 5.0$ km, $\bar{c}_S = 3.7$ km/s, $\delta c_S = 0.2$ km/s, $c_P/c_S = 2$.

SECTION 5

CONCLUSIONS AND FUTURE WORK

In this report we have developed the phase-screen method for elastic vector waves, and demonstrated its use to approximate elastic wave propagation in two dimensions. By comparing with an exact solution we were able to determine the general conditions for which the method is valid. The problem in chapter 3 proved to be quite demanding, particularly on the number of phase screens needed to approximate the exact solution. This was due to the fact that the layered structure allowed only a small number of the modes to propagate for parameters of interest, inducing substantial scattering at oblique angles relative to the direction of propagation of the original wave. For smoother phase distributions, *e. g.* Gaussian phase screens etc., we expect that the method will require fewer phase screens, and may reduce to the usual "parabolic approximation" to produce accurate results.

We also demonstrated how the method may be used to compute P to S conversion in terms of the averaged energy flux. We found that it is energetically more favorable for a P wave to convert its energy into an S wave at a faster rate than for the reverse process, particularly when the longitudinal phase velocity is much larger than the transverse phase velocity. Furthermore, it was demonstrated that the greatest conversion occurs for structure sizes comparable to the P wave wavelength.

The application of the method to a random medium was initiated by randomly aligning the phase screens and ensemble-averaging the results. This provides a genuine first step towards treating a truly random medium problem. The results of the analysis here showed how the energy conversion again proceeds at a faster rate for an initial P wave until the energies reach a fixed asymptotic value. The rate of conversion is proportional to the magnitude of the velocity fluctuations squared, inversely proportional to the structure size, and roughly independent of the frequency for high frequencies. Also, the asymptotic ratio of S wave to P wave energies is approximately given by c_P/c_S. These results indicate that using P–S ratios as a discriminant is viable on regional distance scales of up to 2000 km, provided the velocity perturbations are not too large.

Although this work demonstrates many of the strengths of the phase screen method, it also indicates the need for a great deal of further work to be able to tackle more realistic problems. The following features to be incorporated into the phase-screen framework are under current investigation:

First, the 3D random medium problem with one characteristic length scale is being developed. This will allow $S_H - S_V$ ratios as well as $P-S$ ratios to be computed. Second, the formulation in the time-domain is being developed. This will allow the behavior of transient solutions to be investigated, and the time delay separating the P wave-train from the S wave-train to be computed. Third, we are interested in using sources with spherical symmetry to model explosions. And fourth, the incorporation of phase screens with all length scales represented, weighted according to the PSD of the medium, is under current investigation. This will allow wave propagation through complex realistic media to be stochastically modeled.

The addition of these features should elevate the phase-screen method to the point where it will be a viable tool for seismic discrimination.

SECTION 6

LIST OF REFERENCES

1. Dashen, R., *Path integrals for waves in random media*, J. Math. Phys., 20(5), May 1979.

2. Flatté, S.M. (Editor), *Sound Transmission Through A Fluctuating Ocean*, Cambridge University Press, 1979.

3. Haddon, R.A.W. and E.S. Husebye, *Joint interpretation of P-wave time and amplitude anomalies in terms of lithospheric heterogeneities*, Geophys. J. R. astr. Soc., 55, 19-43, 1978.

4. Knepp, D.L., *Multiple Phase-Screen Calculation of the Temporal Behavior of Stochastic Waves*, Proceedings of the IEEE, Vol. 71, No. 6, June 1983.

5. Martin, J.M. and S.M. Flatté, *Intensity images and statistics from numerical simulation of wave propagation in 3-D random media*, Applied Optics, Vol. 27, No. 11, June 1988.

6. Ratcliffe, J.A., Reports on Progress in Physics, XIX, 190-263, 1956.

7. Wu, R.S. and K. Aki, *Elastic Wave Scattering by a Random Medium and the Small-Scale Inhomogeneities in the Lithosphere*, Journal of Geophysical Research, Vol. 90, No. B12, pp. 10,261-10,273, October 1985.

8. Wu, R.S., *Seismic Wave Scattering*, Article for "Encyclopedia of Geophysics", D.E. James, ed. Van Nostrand Reinhold, September 1988.

Prof. Thomas Ahrens
Seismological Lab, 252-21
Division of Geological & Planetary Sciences
California Institute of Technology
Pasadena, CA 91125

Prof. Charles B. Archambeau
CIRES
University of Colorado
Boulder, CO 80309

Prof. Muawia Barazangi
Institute for the Study of the Continent
Cornell University
Ithaca, NY 14853

Dr. Douglas R. Baumgardt
ENSCO, Inc
5400 Port Royal Road
Springfield, VA 22151-2388

Prof. Jonathan Berger
IGPP, A-025
Scripps Institution of Oceanography
University of California, San Diego
La Jolla, CA 92093

Dr. Lawrence J. Burdick
Woodward-Clyde Consultants
566 El Dorado Street
Pasadena, CA 91109-3245

Dr. Karl Coyner
New England Research, Inc.
76 Olcott Drive
White River Junction, VT 05001

Prof. Vernon F. Cormier
Department of Geology & Geophysics
U-45, Room 207
The University of Connecticut
Storrs, CT 06268

Prof. Steven Day
Department of Geological Sciences
San Diego State University
San Diego, CA 92182

Dr. Zoltan A. Der
ENSCO, Inc.
5400 Port Royal Road
Springfield, VA 22151-2388

Prof. John Ferguson
Center for Lithospheric Studies
The University of Texas at Dallas
P.O. Box 830688
Richardson, TX 75083-0688

Prof. Stanley Flatte
Applied Sciences Building
University of California
Santa Cruz, CA 95064

Dr. Alexander Florence
SRI International
333 Ravenswood Avenue
Menlo Park, CA 94025-3493

Prof. Henry L. Gray
Vice Provost and Dean
Department of Statistical Sciences
Southern Methodist University
Dallas, TX 75275

Dr. Indra Gupta
Teledyne Geotech
314 Montgomery Street
Alexandria, VA 22314

Prof. David G. Harkrider
Seismological Laboratory
Division of Geological & Planetary Sciences
California Institute of Technology
Pasadena, CA 91125

Prof. Donald V. Helmberger
Seismological Laboratory
Division of Geological & Planetary Sciences
California Institute of Technology
Pasadena, CA 91125

Prof. Eugene Herrin
Institute for the Study of Earth and Man
GeophysicalLaboratory
Southern Methodist University
Dallas, TX 75275

Prof. Robert B. Herrmann
Department of Earth & Atmospheric Sciences
St. Louis University
St. Louis, MO 63156

Prof. Bryan Isacks
Cornell University
Department of Geological Sciences
SNEE Hall
Ithaca, NY 14850

Dr. Rong-Song Jih
Teledyne Geotech
314 Montgomery Street
Alexandria, VA 22314

Prof. Lane R. Johnson
Seismographic Station
University of California
Berkeley, CA 94720

Prof. Alan Kafka
Department of Geology & Geophysics
Boston College
Chestnut Hill, MA 02167

Prof. Fred K. Lamb
University of Illinois at Urbana-Champaign
Department of Physics
1110 West Green Street
Urbana, IL 61801

Prof. Charles A. Langston
Geosciences Department
403 Deike Building
The Pennsylvania State University
University Park, PA 16802

Prof. Thorne Lay
Department of Geological Sciences
1006 C.C. Little Building
University of Michigan
Ann Arbor, MI 48109-1063

Prof. Arthur Lerner-Lam
Lamont-Doherty Geological Observatory
of Columbia University
Palisades, NY 10964

Dr. Christopher Lynnes
Teledyne Geotech
314 Montgomery Street
Alexandria, VA 22314

Prof. Peter Malin
University of California at Santa Barbara
Institute for Crustal Studies
Santa Barbara, CA 93106

Dr. Randolph Martin, III
New England Research, Inc.
76 Olcott Drive
White River Junction, VT 05001

Dr. Gary McCartor
Mission Research Corporation
735 State Street
P.O. Drawer 719
Santa Barbara, CA 93102 (2 copies)

Prof. Thomas V. McEvilly
Seismographic Station
University of California
Berkeley, CA 94720

Dr. Keith L. McLaughlin
S-CUBED
A Division of Maxwell Laboratory
P.O. Box 1620
La Jolla, CA 92038-1620

Prof. William Menke
Lamont-Doherty Geological Observatory
of Columbia University
Palisades, NY 10964

Stephen Miller
SRI International
333 Ravenswood Avenue
Box AF 116
Menlo Park, CA 94025-3493

Prof. Bernard Minster
IGPP, A-025
Scripps Institute of Oceanography
University of California, San Diego
La Jolla, CA 92093

Prof. Brian J. Mitchell
Department of Earth & Atmospheric Sciences
St. Louis University
St. Louis, MO 63156

Mr. Jack Murphy
S-CUBED, A Division of Maxwell Laboratory
11800 Sunrise Valley Drive
Suite 1212
Reston, VA 22091 (2 copies)

Dr. Bao Nguyen
GL/LWH
Hanscom AFB, MA 01731-5000

Prof. John A. Orcutt
IGPP, A-025
Scripps Institute of Oceanography
University of California, San Diego
La Jolla, CA 92093

Prof. Keith Priestley
University of Nevada
Mackay School of Mines
Reno, NV 89557

Prof. Paul G. Richards
Lamont-Doherty Geological Observatory
of Columbia University
Palisades, NY 10964

Dr. Wilmer Rivers
Teledyne Geotech
314 Montgomery Street
Alexandria, VA 22314

Dr. Alan S. Ryall, Jr.
Center for Seismic Studies
1300 North 17th Street
Suite 1450
Arlington, VA 22209-2308

Prof. Charles G. Sammis
Center for Earth Sciences
University of Southern California
University Park
Los Angeles, CA 90089-0741

Prof. Christopher H. Scholz
Lamont-Doherty Geological Observatory
of Columbia University
Palisades, NY 10964

Prof. David G. Simpson
Lamont-Doherty Geological Observatory
of Columbia University
Palisades, NY 10964

Dr. Jeffrey Stevens
S-CUBED
A Division of Maxwell Laboratory
P.O. Box 1620
La Jolla, CA 92038-1620

Prof. Brian Stump
Institute for the Study of Earth & Man
Geophysical Laboratory
Southern Methodist University
Dallas, TX 75275

Prof. Jeremiah Sullivan
University of Illinois at Urbana-Champaign
Department of Physics
1110 West Green Street
Urbana, IL 61801

Prof. Clifford Thurber
University of Wisconsin-Madison
Department of Geology & Geophysics
1215 West Dayton Street
Madison, WS 53706

Prof. M. Nafi Toksoz
Earth Resources Lab
Massachusetts Institute of Technology
42 Carleton Street
Cambridge, MA 02142

Prof. John E. Vidale
University of California at Santa Cruz
Seismological Laboratory
Santa Cruz, CA 95064

Prof. Terry C. Wallace
Department of Geosciences
Building #77
University of Arizona
Tucson, AZ 85721

Dr. Raymond Willeman
GL/LWH
Hanscom AFB, MA 01731-5000

Dr. Lorraine Wolf
GL/LWH
Hanscom AFB, MA 01731-5000

Prof. Francis T. Wu
Department of Geological Sciences
State University of New York
at Binghamton
Vestal, NY 13901

Dr. Monem Abdel-Gawad
Rockwell International Science Center
1049 Camino Dos Rios
Thousand Oaks, CA 91360

Prof. Keiiti Aki
Center for Earth Sciences
University of Southern California
University Park
Los Angeles, CA 90089-0741

Prof. Shelton S. Alexander
Geosciences Department
403 Deike Building
The Pennsylvania State University
University Park, PA 16802

Dr. Ralph Archuleta
Department of Geological Sciences
University of California at Santa Barbara
Santa Barbara, CA 93102

Dr. Thomas C. Bache, Jr.
Science Applications Int'l Corp.
10210 Campus Point Drive
San Diego, CA 92121 (2 copies)

J. Barker
Department of Geological Sciences
State University of New York
at Binghamton
Vestal, NY 13901

Dr. T.J. Bennett
S-CUBED
A Division of Maxwell Laboratory
11800 Sunrise Valley Drive, Suite 1212
Reston, VA 22091

Mr. William J. Best
907 Westwood Drive
Vienna, VA 22180

Dr. N. Biswas
Geophysical Institute
University of Alaska
Fairbanks, AK 99701

Dr. G.A. Bollinger
Department of Geological Sciences
Virginia Polytechnical Institute
21044 Derring Hall
Blacksburg, VA 24061

Dr. Stephen Bratt
Science Applications Int'l Corp.
10210 Campus Point Drive
San Diego, CA 92121

Michael Browne
Teledyne Geotech
3401 Shiloh Road
Garland, TX 75041

Mr. Roy Burger
1221 Serry Road
Schenectady, NY 12309

Dr. Robert Burridge
Schlumberger-Doll Research Center
Old Quarry Road
Ridgefield, CT 06877

Dr. Jerry Carter
Rondout Associates
P.O. Box 224
Stone Ridge, NY 12484

Dr. W. Winston Chan
Teledyne Geotech
314 Montgomery Street
Alexandria, VA 22314-1581

Dr. Theodore Cherry
Science Horizons, Inc.
710 Encinitas Blvd., Suite 200
Encinitas, CA 92024 (2 copies)

Prof. Jon F. Claerbout
Department of Geophysics
Stanford University
Stanford, CA 94305

Prof. Robert W. Clayton
Seismological Laboratory
Division of Geological & Planetary Sciences
California Institute of Technology
Pasadena, CA 91125

Prof. F. A. Dahlen
Geological and Geophysical Sciences
Princeton University
Princeton, NJ 08544-0636

-4-

Prof. Anton W. Dainty
Earth Resources Lab
Massachusetts Institute of Technology
42 Carleton Street
Cambridge, MA 02142

Prof. Adam Dziewonski
Hoffman Laboratory
Harvard University
20 Oxford St
Cambridge, MA 02138

Prof. John Ebel
Department of Geology & Geophysics
Boston College
Chestnut Hill, MA 02167

Eric Fielding
SNEE Hall
INSTOC
Cornell University
Ithaca, NY 14853

Prof. Donald Forsyth
Department of Geological Sciences
Brown University
Providence, RI 02912

Prof. Art Frankel
Mail Stop 922
Geological Survey
790 National Center
Reston, VA 22092

Dr. Anthony Gangi
Texas A&M University
Department of Geophysics
College Station, TX 77843

Dr. Freeman Gilbert
Inst. of Geophysics & Planetary Physics
University of California, San Diego
P.O. Box 109
La Jolla, CA 92037

Mr. Edward Giller
Pacific Sierra Research Corp.
1401 Wilson Boulevard
Arlington, VA 22209

Dr. Jeffrey W. Given
Sierra Geophysics
11255 Kirkland Way
Kirkland, WA 98033

Prof. Stephen Grand
University of Texas at Austin
Department of Geological Sciences
Austin, TX 78713-7909

Prof. Roy Greenfield
Geosciences Department
403 Deike Building
The Pennsylvania State University
University Park, PA 16802

Dan N. Hagedorn
Battelle
Pacific Northwest Laboratories
Battelle Boulevard
Richland, WA 99352

Kevin Hutchenson
Department of Earth Sciences
St. Louis University
3507 Laclede
St. Louis, MO 63103

Prof. Thomas H. Jordan
Department of Earth, Atmospheric
  and Planetary Sciences
Massachusetts Institute of Technology
Cambridge, MA 02139

Robert C. Kemerait
ENSCO, Inc.
445 Pineda Court
Melbourne, FL 32940

William Kikendall
Teledyne Geotech
3401 Shiloh Road
Garland, TX 75041

Prof. Leon Knopoff
University of California
Institute of Geophysics & Planetary Physics
Los Angeles, CA 90024

Prof. L. Timothy Long
School of Geophysical Sciences
Georgia Institute of Technology
Atlanta, GA 30332

Prof. Art McGarr
Mail Stop 977
Geological Survey
345 Middlefield Rd.
Menlo Park, CA 94025

Dr. George Mellman
Sierra Geophysics
11255 Kirkland Way
Kirkland, WA 98033

Prof. John Nabelek
College of Oceanography
Oregon State University
Corvallis, OR 97331

Prof. Geza Nagy
University of California, San Diego
Department of Ames, M.S. B-010
La Jolla, CA 92093

Prof. Amos Nur
Department of Geophysics
Stanford University
Stanford, CA 94305

Prof. Jack Oliver
Department of Geology
Cornell University
Ithaca, NY 14850

Prof. Robert Phinney
Geological & Geophysical Sciences
Princeton University
Princeton, NJ 08544-0636

Dr. Paul Pomeroy
Rondout Associates
P.O. Box 224
Stone Ridge, NY 12484

Dr. Jay Pulli
RADIX System, Inc.
2 Taft Court, Suite 203
Rockville, MD 20850

Dr. Norton Rimer
S-CUBED
A Division of Maxwell Laboratory
P.O. Box 1620
La Jolla, CA 92038-1620

Prof. Larry J. Ruff
Department of Geological Sciences
1006 C.C. Little Building
University of Michigan
Ann Arbor, MI 48109-1063

Dr. Richard Sailor
TASC Inc.
55 Walkers Brook Drive
Reading, MA 01867

Thomas J. Sereno, Jr.
Science Application Int'l Corp.
10210 Campus Point Drive
San Diego, CA 92121

John Sherwin
Teledyne Geotech
3401 Shiloh Road
Garland, TX 75041

Prof. Robert Smith
Department of Geophysics
University of Utah
1400 East 2nd South
Salt Lake City, UT 84112

Prof. S. W. Smith
Geophysics Program
University of Washington
Seattle, WA 98195

Dr. Stewart Smith
IRIS Inc.
1616 North Fort Myer Drive
Suite 1440
Arlington, VA 22209

Dr. George Sutton
Rondout Associates
P.O. Box 224
Stone Ridge, NY 12484

Prof. L. Sykes
Lamont-Doherty Geological Observatory
of Columbia University
Palisades, NY 10964

Prof. Pradeep Talwani
Department of Geological Sciences
University of South Carolina
Columbia, SC 29208

Prof. Ta-liang Teng
Center for Earth Sciences
University of Southern California
University Park
Los Angeles, CA 90089-0741

-6-

Dr. R.B. Tittmann
Rockwell International Science Center
1049 Camino Dos Rios
P.O. Box 1085
Thousand Oaks, CA 91360

Dr. Gregory van der Vink
IRIS, Inc.
1616 North Fort Myer Drive
Suite 1440
Arlington, VA 22209

William R. Walter
Seismological Laboratory
University of Nevada
Reno, NV 89557

Dr. Gregory Wojcik
Weidlinger Associates
4410 El Camino Real
Suite 110
Los Altos, CA 94022

Prof. John H. Woodhouse
Hoffman Laboratory
Harvard University
20 Oxford Street
Cambridge, MA 02138

Dr. Gregory B. Young
ENSCO, Inc.
5400 Port Royal Road
Springfield, VA 22151-2388

Dr. Ralph Alewine III
DARPA/NMRO
1400 Wilson Boulevard
Arlington, VA 01731-5000

Paul Johnson
ESS-4, Mail Stop J979
Los Alamos National Laboratory
Los Alamos, NM 87545

Mr. James C. Battis
GL/LWH
Hanscom AFB, MA 22209-2308

Janet Johnston
GL/LWH
Hanscom AFB, MA 01731-5000

Dr. Robert Blandford
DARPA/NMRO
1400 Wilson Boulevard
Arlington, VA 87185

Dr. Katharine Kadinsky-Cade
GL/LWH
Hanscom AFB, MA 01731-5000

Eric Chael
Division 9241
Sandia Laboratory
Albuquerque, NM 01731-5000

Ms. Ann Kerr
IGPP, A-025
Scripps Institute of Oceanography
University of California, San Diego
La Jolla, CA 92093

Dr. John J. Cipar
GL/LWH
Hanscom AFB, MA 01731-5000

Dr. Max Koontz
US Dept of Energy/DP 5
Forrestal Building
1000 Independence Avenue
Washington, DC 20585

Mr. Jeff Duncan
Office of Congressman Markey
2133 Rayburn House Bldg.
Washington, D.C. 20515

Dr. W.H.K. Lee
Office of Earthquakes, Volcanoes,
& Engineering
345 Middlefield Road
Menlo Park, CA 94025

Dr. Jack Evernden
USGS - Earthquake Studies
345 Middlefield Road
Menlo Park, CA 94025

Dr. William Leith
U.S. Geological Survey
Mail Stop 928
Reston, VA 22092

Art Frankel
USGS
922 National Center
Reston, VA 22092

Dr. Richard Lewis
Director, Earthquake Engineering & Geophysics
U.S. Army Corps of Engineers
Box 631
Vicksburg, MS 39180

Dr. T. Hanks
USGS
Nat'l Earthquake Research Center
345 Middlefield Road
Menlo Park, CA 94025

James F. Lewkowicz
GL/LWH
Hanscom AFB, MA 01731-5000

Dr. James Hannon
Lawrence Livermore Nat'l Laboratory
P.O. Box 808
Livermore, CA 94550

Mr. Alfred Lieberman
ACDA/VI-OA State Department Bldg
Room 5726
320 - 21st Street, NW
Washington, DC 20451

-8-

Stephen Mangino
GL/LWH
Hanscom AFB, MA 01731-5000

Dr. Frank F. Pilotte
HQ AFTAC/TT
Patrick AFB, FL. 32925-6001

Dr. Robert Masse
Box 25046, Mail Stop 967
Denver Federal Center
Denver, CO 80225

Katie Poley
CIA-OSWR/NED
Washington, DC 20505

Art McGarr
U.S. Geological Survey, MS-977
345 Middlefield Road
Menlo Park, CA 94025

Mr. Jack Rachlin
U.S. Geological Survey
Geology, Rm 3 C136
Mail Stop 928 National Center
Reston, VA 22092

Richard Morrow
ACDA/VI, Room 5741
320 21st Street N.W
Washington, DC 20451

Dr. Robert Reinke
WL/NTESG
Kirtland AFB, NM 87117-6008

Dr. Keith K. Nakanishi
Lawrence Livermore National Laboratory
P.O. Box 808, L-205
Livermore, CA 94550

Dr. Byron Ristvet
HQ DNA, Nevada Operations Office
Attn: NVCG
P.O. Box 98539
Las Vegas, NV 89193

Dr. Carl Newton
Los Alamos National Laboratory
P.O. Box 1663
Mail Stop C335, Group ESS-3
Los Alamos, NM 87545

Dr. George Rothe
HQ AFTAC/TGR
Patrick AFB, FL 32925-6001

Dr. Kenneth H. Olsen
Los Alamos Scientific Laboratory
P.O. Box 1663
Mail Stop C335, Group ESS-3
Los Alamos, NM 87545

Dr. Michael Shore
Defense Nuclear Agency/SPSS
6801 Telegraph Road
Alexandria, VA 22310

Howard J. Patton
Lawrence Livermore National Laboratory
P.O. Box 808, L-205
Livermore, CA 94550

Donald L. Springer
Lawrence Livermore National Laboratory
P.O. Box 808, L-205
Livermore, CA 94550

Mr. Chris Paine
Office of Senator Kennedy, SR 315

United States Senate
Washington, DC 20510

Dr. Lawrence Turnbull
OSWR/NED
Central Intelligence Agency, Room 5G48
Washington, DC 20505

Colonel Jerry J. Perrizo
AFOSR/NP, Building 410
Bolling AFB
Washington, DC 20332-6448

Dr. Thomas Weaver
Los Alamos National Laboratory
P.O. Box 16('lail Stop C335
Los Alamos, .. 87545

Dr. Ramon Cabre, S.J.
Observatorio San Calixto
Casilla 5939
La Paz, Bolivia

Prof. Hans-Peter Harjes
Institute for Geophysik
Ruhr University/Bochum
P.O. Box 102148
4630 Bochum 1, FRG

Prof. Eystein Husebye
NTNF/NORSAR
P.O. Box 51
N-2007 Kjeller, NORWAY

Prof. Brian L.N. Kennett
Research School of Earth Sciences
Institute of Advanced Studies
G.P.O. Box 4
Canberra 2601, AUSTRALIA

Dr. Bernard Massinon
Societe Radiomana
27 rue Claude Bernard
75005 Paris, FRANCE (2 Copies)

Dr. Pierre Mecheler
Societe Radiomana
27 rue Claude Bernard
75005 Paris, FRANCE

Dr. Svein Mykkeltveit
NTNF/NORSAR
P.O. Box 51
N-2007 Kjeller, NORWAY

Dr. Peter Basham
Earth Physics Branch
Geological Survey of Canada
1 Observatory Crescent
Ottawa, Ontario, CANADA K1A 0Y3

Dr. Eduard Berg
Institute of Geophysics
University of Hawaii
Honolulu, HI 96822

Dr. Michel Bouchon
I.R.I.G.M.-B.P. 68
38402 St. Martin D'Heres
Cedex, FRANCE

Dr. Hilmar Bungum
NTNF/NORSAR
P.O. Box 51
N-2007 Kjeller, NORWAY

Dr. Michel Campillo
Observatoire de Grenoble
I.R.I.G.M -   3
38041 Grenoble, FRANCE

Dr. Kin Yip Chun
Geophysics Division
Physics Department
University of Toronto
Ontario, CANADA M5S 1A7

Dr. Alan Douglas
Ministry of Defense
Blacknest, Brimpton
Reading RG7-4RS, UNITED KINGDOM

Dr. Roger Hansen
NTNF/NORSAR
P.O. Box 51
N-2007 Kjeller, NORWAY

Dr. Manfred Henger
Federal Institute for Geosciences & Nat'l Res.
Postfach 510153
D-3000 Hanover 51, FRG

Ms. Eva Johannisson
Senior Research Officer
National Defense Research Inst.
P.O. Box 27322
S-102 54 Stockholm, SWEDEN

Dr. Fekadu Kebede
Seismological Section
Box 12019
S-750 Uppsala, SWEDEN

Dr. Tormod Kvaerna
NTNF/NORSAR
P.O. Box 51
N-2007 Kjeller, NORWAY

Dr. Peter Marshal
Procurement Executive
Ministry of Defense
Blacknest, Brimpton
Reading FG7-4RS, UNITED KINGDOM

Prof. Ari Ben-Menahem
Department of Applied Mathematics
Weizman Institute of Science
Rehovot, ISRAEL 951729

Dr. Robert North
Geophysics Division
Geological Survey of Canada
1 Observatory Crescent
Ottawa, Ontario, CANADA K1A 0Y3

Dr. Frode Ringdal
NTNF/NORSAR
P.O. Box 51
N-2007 Kjeller, NORWAY

Dr. Jorg Schlittenhardt
Federal Institute for Geosciences & Nat'l Res.
Postfach 510153
D-3000 Hannover 51, FEDERAL REPUBLIC OF
GERMANY

Prof. Daniel Walker
University of Hawaii
Institute of Geophysics
Honolulu, HI 96822